Driving proteomic imbalance in malignancy provokes proteomic catastrophe and confers tumor suppression

Babul Moni Ram[1], Omprakash Shriwas[1], Meng Xu[1], Kun-Han Chuang[1,2], and Chengkai Dai[1,*]

[1]Mouse Cancer Genetics Program, Center for Cancer Research, National Cancer Institute, Frederick, MD 21702, USA

[2]Present address: School of Basic Medical Sciences, Fujian Medical University, Fuzhou, Fujian 350108, China

*Correspondence: Chengkai.dai@nih.gov

ABSTRACT

Unlike genomic instability, the implications of proteomic instability in cancer remain ambiguous. By governing the proteotoxic stress response, heat shock factor 1 (HSF1) sustains proteomic stability upon environmental insults. Apart from its importance to stress resistance and survival, HSF1 is emerging as a powerful oncogenic enabler. In the Neurofibromatosis type I (*NF1*)-deficient malignant peripheral nerve sheath tumor (MPNST) cells, *HSF1* depletion triggered protein polyubiquitination, aggregation, and even tumor-suppressive amyloidogenesis. In contrast, *HSF1* is dispensable for the proteome of non-transformed human Schwann cells. Mechanistically, HSF1 defends the essential mitochondrial chaperone HSP60 against the direct assault from soluble amyloid oligomers. To survive and adapt to compromised protein quality, owing to *HSF1* deficiency, MPNST cells mobilized JNK to repress mTORC1 and protein translation, thereby attenuating protein quantity to alleviate proteomic imbalance. mTORC1 stimulation, via either pharmacological JNK blockade, genetic *TSC2* depletion, or leucine supplementation, markedly aggravated the proteomic imbalance elicited by *HSF1* deficiency. This catastrophic imbalance instigated pronounced cell death partly through unchecked amyloidogenesis, thereby exerting tumor suppression in both MPNST and melanoma models *in vivo*. Thus, HSF1 safeguards the cancer proteome to enable the oncogenic potential of mTORC1. This proof-of-principle study highlights provoking proteomic catastrophe as a next-generation therapeutic concept for combating malignancy.

INTRODUCTION

Compared to genomic instability, proteomic instability in cancer is underappreciated. Malignant transformation prompts proteotoxic stress and destabilizes the proteome.[1, 2] Several mechanisms, including reactive oxygen species, genetic mutations, and uncontrolled protein translation, all lead to increased protein damage, misfolding, as well as aggregation.[1-3] Of great interest, amyloidogenesis, a hallmark of neurodegenerative disorders,[4] also occurs in cancer.[5] Unlike neurons, cancerous cells manage to contain amyloidogenesis and counteract the cytotoxic effects of amyloids. Among various cellular anti-amyloid mechanisms is heat shock factor 1 (HSF1) and its mediated heat shock response or proteotoxic stress response (HSR/PSR), a powerful cytoprotective transcriptional program.[6-8] In accordance with its role in repressing proteomic instability, HSF1 has emerged as a potent oncogenic enabler, independently of driver mutations.[9-15]

Sharply contrasting with its dispensability for primary and non-transformed cells, HSF1 becomes essential to numerous cancer cell lines,[9,13,16-18] owing to their elevated intrinsic proteotoxic stress. This phenomenon is referred to as "HSF1 or non-oncogene addiction of cancer",[2,19] justifying HSF1 as a promising therapeutic target.

Neurofibromatosis type 1 (NF1) is a cancer predisposition syndrome afflicting approximately 1 in 3000 individuals worldwide.[20] About 30-50% of NF1 individuals develop benign plexiform neurofibromas, which, unlike dermal neurofibromas, can transform into highly aggressive malignant peripheral nerve sheath tumors (MPNSTs) with poor prognosis and survival.[21] The *NF1* gene encodes neurofibromin, a 250-280 kDa RAS GTPase activating protein (GAP) that

negatively regulates RAS activity.[22] *NF1* inactivation in MPNST cells dysregulates RAS/MAPK signaling which, in addition to stimulating cell growth, leads to constitutive HSF1 activation.[13] Concomitantly, HSF1 overexpression and activation are seen in both *in vitro* and *in vivo* MPNST models as well as primary NF1 tumors.[13] Importantly, *Hsf1* deficiency impaired the NF1-associated tumorigenesis in mice in part by attenuating oncogenic RAS signaling.[13]

Utilizing the NF1 tumor model system, we herein demonstrate HSF1 as a key player in countering proteomic instability in cancer. We discover that amyloidogenesis occurs in *NF1*-deficient MPNST cells, partly due to hyperactive mTORC1 and augmented protein translation. HSF1 inhibition destabilizes the cancer proteome, promoting global protein polyubiquitination, aggregation, as well as amyloidogenesis. Importantly, this proteomic instability causes cytotoxicity. To adapt and survive HSF1 inhibition, MPNST cells mobilize JNK to suppress mTORC1 and thereby mitigate protein translation. Disrupting this adaptative response through JNK inhibition aggravates amyloidogenesis and cytotoxicity. Similarly, mTORC1 stimulation, via either genetic *TSC2* depletion or supplementation with leucine or its analog, synergizes with HSF1 inhibition to inflict profound proteomic chaos and widespread non-apoptotic cell death. Of note, blockade of amyloidogenesis markedly alleviates cell death. Thus, our findings illuminate a prominent role of HSF1 in antagonizing proteomic instability in cancerous cells, constituting a generic pro-oncogenic mechanism. This study exemplifies a proof of principle and, importantly, institutes provoking proteomic catastrophe as a next-generation anti-cancer therapeutic concept.

RESULTS

HSF1 counters proteomic instability in *NF1*-deficient MPNST cells

Previously, we found that loss of *NF1* leads to constitutive activation of HSF1 and that *Hsf1* deficiency impairs the tumorigenesis in *Nf1*$^{+/-}$; *p53*$^{+/-}$ (NPcis) mice.[13] In human cancers, *NF1* deletion is associated with elevated *HSF1* gene expression (Figure 1A). Moreover, the expression of *NF1* and *HSF1* genes are inversely correlated in human cancers (Figure S1A). Importantly, among patients whose tumors harbor *NF1* deletion higher *HSF1* expression is correlated with shortened survival (Figure 1B). Collectively, these findings support a pro-oncogenic role of HSF1 in *NF1*-deficient malignancies.

Given its critical role in governing protein folding, we were curious about how *HSF1* depletion impacts the proteomes of *NF1*-deficient MPNST cells as well as *NF1*-proficient non-transformed human Schwann cells (HSCs), both primary and immortalized. HSCs are considered as the cell-of-origin of MPNSTs.[20,22] In three different MPNST cell lines (90-8TL, S462, and SNF96.2), transient depletion of *HSF1*, using two previously validated lentiviral shRNAs,[9,13] all caused an increase in global protein Lys48-specific polyubiquitination, a molecular mark for proteasomal degradation,[23] in both detergent-soluble and -insoluble fractions (Figures 1C, 1D, S1B, and S1C). This increased polyubiquitination signifies proteome-wide misfolding and aggregation. In stark contrast, this change was not observed in HSCs (Figures 1C and 1D). Thus, *HSF1* depletion provokes proteomic instability in MPNST cells, but not in HSCs.

Most cellular protein aggregates are amorphous; however, a tiny fraction becomes highly ordered and enriched with β-sheet structures. These special protein aggregates, namely amyloids, are

116 closely associated with neurodegenerative disorders in humans, especially Alzheimer's disease.[24]
117 To assess whether *HSF1* depletion could elicit amyloidogenesis, we stained both MPNST cells and
118 HSCs with Congo red (CR), a widely applied amyloid-binding fluorescent dye.[25] Compared to
119 HSCs, MPNST cells displayed more intense CR staining (Figure 1E), suggesting increased
120 amyloids in malignant Schwann cells. Importantly, *HSF1* depletion further intensified CR staining
121 in MPNST cells, but not in HSCs (Figures 1E, 1F, S1D, and S1E). Similar results were obtained
122 by Thioflavin T staining (Figure S1F), another popular amyloid dye.[25] Importantly, the induction
123 of amyloids was further confirmed by ELISA using two conformation-specific antibodies (A11
124 and OC), which recognize soluble amyloid oligomers (AOs) and insoluble amyloid fibrils (AFs),
125 respectively.[26,27] Upon *HSF1* depletion, all three MPNST cell lines displayed elevated levels of
126 $A11^+$ AOs and OC^+ AFs (Figures 1G, 1H, S1G-S1J). Again, no evident increase in amyloids was
127 detected in HSCs (Figures 1I and 1J). Together, these findings indicate that HSF1 is required to
128 safeguard the proteome of malignant Schwann cells and particularly to repress amyloidogenesis;
129 on the contrary, it is dispensable for the proteome of non-transformed Schwann cells.
130
131 **Unchecked proteomic instability is tumor suppressive**
132 It has become evident that HSF1 acts as a generic oncogenic enabler; nevertheless, a universal
133 underlying mechanism remains undefined.
134
135 A healthy proteome enables the translation of genotypes into phenotypes. Thus, we reasoned that
136 preservation of proteomic stability is most likely a generic pro-oncogenic mechanism of HSF1.
137 To test this notion, we first determined whether proteomic instability, particularly
138 amyloidogenesis, is causally related to the cytotoxicity induced by *HSF1* depletion in cancer

139 cells. To block amyloidogenesis we employed CR, which is known to exert anti-amyloid effects
140 through its amyloid-binding activity.[5,28,29] Consistent with "HSF1 addiction of cancer", *HSF1*
141 depletion markedly impaired the viability of MPNST cells; importantly, CR treatment partially
142 rescued this impaired viability (Figures 2A, S2A, and S2B). In contrast, both *HSF1* depletion and
143 CR treatment did not affect HSCs (Figure 2B), congruent with a lack of proteomic instability and
144 amyloidogenesis in these non-transformed cells. Together, these findings support that unchecked
145 proteomic instability, particularly amyloidogenesis, is cytotoxic and tumor suppressive.
146 Moreover, HSF1 enables oncogenesis in part by constraining proteomic instability.
147
148 **HSF1 neutralizes soluble amyloid oligomers to protect MPNST cells**
149 Then, how does HSF1 counter amyloids to enable the growth and survival of MPNST cells?
150 Recently, by researching tissue overgrowth models we discovered that HSF1, surprisingly,
151 physically neutralizes soluble AOs, thereby preventing their assault on HSP60.[30] As an essential
152 mitochondrial chaperone, HSP60 functions as a guardian of the mitochondrial proteome.[30-32]
153
154 We wondered whether HSF1 acts the same way in both cancer and tissue overgrowth. Co-IP
155 experiments indicated that $A11^+$ AOs physically interacted with HSF1, but not major HSPs, in
156 MPNST cells (Figure 2C), consistent with our findings in tissue overgrowth models.[30] This AO-
157 HSF1 interaction was further validated by another independent technique, *in situ* Proximity
158 Ligation Assay (PLA) (Figures 2D-2F). Importantly, *HSF1* depletion promoted the AO-HSP60
159 interaction (Figure 2G and 2H). Loss of *HSP60* destabilized the mitochondrial proteome.[30,32]
160 Thus, this AO-HSP60 interaction signifies the instigation of mitochondrial damage and

161 cytotoxicity. Taken together, our findings reveal that HSF1 protects MPNST cells in part by
162 neutralizing soluble AOs to safeguard HSP60 and the mitochondrial proteome (Figure 2I).
163
164 **MPNST cells react to HSF1 deficiency by activating JNK to attenuate translation**
165 Given their dependency on HSF1, cancer cells are expected to mount certain responses to
166 survive and adapt to the lethal HSF1 inhibition. Previously, we uncovered that in *Hsf1*-deficient
167 mice, the stress-responsive JNK kinase becomes constitutively activated, which, in turn,
168 disassembles mTORC1.[33] JNK does so by phosphorylating both RAPTOR and mTOR, two core
169 components of mTORC1. This mTORC1 inhibition diminishes protein translation, leading to
170 reduced cell size and whole-body lean mass in *Hsf1*-deficient mice.[33]
171
172 We reasoned that cancer cells might exploit this molecular regulation for their survival and
173 adaptation. In MPNST cells *HSF1* knockdown activated JNK, indicated by elevated JNK
174 T183/Y185 phosphorylation; in parallel to JNK activation, there was mTORC1 inhibition,
175 evidenced by diminished p70S6K T389 phosphorylation and 4EBP1 S65/T70 phosphorylation
176 (Figures 3A, 3B, and S3A-S3D).[34,35] In contrast, *HSF*1 knockdown minimally affected JNK and
177 mTORC1 in HSCs (Figures 3A and 3B). Detected by PLA, in MPNST cells HSF1 interacted
178 with JNK; however, *HSF1* depletion promoted JNK-RAPTOR interactions but diminished
179 mTOR-RAPTOR interactions simultaneously (Figures 3C-3E). The mTOR-RAPTOR interaction
180 is essential to the assembly and activity of mTORC1.[36] Thus, these findings support that JNK
181 senses HSF1 deficiency to repress mTORC1. Of interest, compared to non-transformed cells,
182 this sensing mechanism appears more prominent in malignant cells.
183

184 As expected for mTORC1 inhibition, *HSF1* depletion reduced global protein translation rate in
185 MPNST cells (Figures 3F, S3E, and S3F), detected by puromycin labeling as described
186 previously.[33,37] Beyond MPNST cells, this regulation of translation by HSF1 was conserved in
187 diverse human cancer cell lines (Figure 3G). Importantly, treatment with JNK-IN-8, an
188 irreversible JNK inhibitor,[38] largely rescued this impaired protein translation owing to *HSF1*
189 depletion (Figures 3F, S3E, and S3F). Interestingly, JNK inhibition augmented the basal
190 translation rate as well. Consistent with these findings, in human cancers higher *HSF1*
191 expression is associated with lower JNK activation (Figure S3G); in turn, lower JNK activation
192 is accompanied by higher mTORC1 activity, reflected by higher 4EBP1 Ser65 phosphorylation
193 (Figure S3H). In aggregate, our findings demonstrate that JNK activation is causally linked to
194 inhibition of mTORC1 and translation. Therefore, through JNK suppression HSF1 permits
195 robust protein translation, which is fundamental to malignant growth (Figure 3H).
196
197 **Lessening protein quantity is an adaptive response to alleviate proteomic instability**
198 We next asked why cells respond to HSF1 deficiency by attenuating translation. While HSF1
199 controls protein quality via HSPs, mTORC1 governs protein quantity via translation. It would be
200 beneficial to lower protein quantity when protein quality is jeopardized. Thus, we reasoned that
201 this regulation might represent a cellular adaptive response to imbalanced protein quantity and
202 quality engendered by HSF1 deficiency.
203
204 Proteomic imbalance disrupts proteome homeostasis and contributes to proteomic instability,
205 which may ultimately trigger amyloidogenesis. To inflict proteomic imbalance, we first
206 stimulated protein translation in MPNST cells by inhibiting JNK. As expected, JNK-IN-8

207 reduced the phosphorylation of c-JUN, a canonical substrate of JNK,[34] in MPNST cells (Figure
208 4A). In support of enhanced protein translation, JNK-IN-8 further activated mTORC1 in these
209 cells (Figures 4A and S4A); in contrast, marginal effects were observed in HSCs (Figure 4B).
210 Congruently, JNK-IN-8 did not significantly reduce c-JUN phosphorylation in HSCs, supporting
211 a lack of JNK activation in these non-transformed Schwann cells. Intriguingly, the heightened
212 protein translation following JNK inhibition was accompanied by elevated amyloid levels in
213 MPNST cells (Figures 4C and S4B). On the contrary, there were no significant changes in
214 amyloid levels in HSCs (Figure 4D).
215
216 To determine the role of protein translation in amyloidogenesis, we chose to block translation
217 using two pharmacological inhibitors, 4EGI-1 and LY2584702, with distinct mechanisms of
218 action. While 4EGI-1 disrupts eIF4E-eIF4G interactions,[39] LY2584702 inhibits p70S6K.[40]
219 Interestingly, both inhibitors diminished the basal amyloid levels in MPNST cells (Figures
220 4E,4F, and S4C), revealing a causal relationship between protein translation and
221 amyloidogenesis. Importantly, translation inhibition also blocked the induction of amyloids by
222 JNK-IN-8 in MPNST cells (Figures 4G, 4H, S4D, and S4E), indicating that JNK suppresses
223 amyloidogenesis via translation inhibition. No significant effects were observed in HSCs
224 (Figures 4G and 4H).
225
226 Considering the role of translation in amyloidogenesis, we reasoned that preventing translation
227 attenuation would aggravate proteomic imbalance and enhance cytotoxicity in malignant cells.
228 As expected, JNK-IN-8 further elevated the amyloid levels in MPNST cells following *HSF1*
229 depletion, which was accompanied by exacerbated apoptosis, detected by caspase 3 cleavage

230 (Figures 4I, 4J, and S4F).[41] Importantly, CR treatment blocked apoptosis, detected by PARP
231 cleavage (Figure S4G),[42] causally implicating amyloidogenesis. In contrast, *HSF1* depletion and
232 JNK inhibition exerted no significant impacts on non-transformed Schwann cells (Figures 4K
233 and 4L). Thus, our findings support that proteomic imbalance in malignant cells contributes to
234 proteomic instability and amyloidogenesis. In stark contrast, there is no or little amyloidogenesis
235 in non-transformed cells, owing to their balanced protein quantity and quality. Moreover,
236 through translation attenuation, malignant cells attempt to survive and adapt to proteomic
237 imbalance (Figure 4M).
238
239 **mTORC1 stimulation aggravates proteomic imbalance and cytotoxicity induced by HSF1**
240 **inhibition**
241 JNK regulates numerous targets other than mTORC1. To stimulate mTORC1 and protein
242 translation specifically, we next genetically inhibited the tumor suppressor Tuberous Sclerosis
243 Complex subunit 2 (*TSC2*), a key negative regulator of mTORC1,[43] in MPNST cells. As
244 expected, knocking down *TSC2* in MPNST cells promoted phosphorylation of both p70S6K and
245 4EBP1, which was accompanied by elevated amyloids (Figures S5A-S5F). Like genetic *HSF1*
246 depletion, pharmacological inhibition of HSF1 by DTHIB elevated global protein
247 polyubiquitination and amyloids in MPNST cells (Figures 5A, 5B, and S5G), eliciting proteomic
248 instability. The newly developed small-molecule inhibitor DTHIB directly binds to the DNA-
249 binding domain of HSF1 and potently blocks the HSF1-mediated transcription.[44] Compared to
250 control cells, HSF1 inhibition by DTHIB induced considerably higher levels of amyloids in
251 *TSC2*-deficient MPNST cells (Figure 5B). Of note, *TSC2*-deficient cells displayed more
252 profound JNK activation and mTORC1 inhibition following DTHIB treatment, reflecting an

253 intensified cellular response to severe proteotoxic stress. Consistently, compared to slight or
254 intermediate cytotoxicity in control MPNST cells, detected by plasma membrane
255 permeabilization, *TSC2*-deficient cells were highly sensitive to HSF1 inhibition (Figures 5C, 5D,
256 and S5H-S5K). Importantly, either translation inhibition or CR treatment largely blocked this
257 cytotoxicity (Figures 5C and 5D), causally implicating proteomic instability and
258 amyloidogenesis. In support of a role of HSF1 in enabling *TSC2* deficiency, among patients
259 whose tumors harbor *TSC2* deletion higher *HSF1* gene expression is correlated with shortened
260 survival (Figure S5L).
261
262 To exclude possible mTORC1-independent effects of *TSC2* deficiency, we alternatively fed cells
263 with NV-5138, a leucine analog currently under clinical trials as an antidepressant.[45,46]Amino
264 acids, particularly leucine, are potent activators of mTORC1.[47] Of interest, whereas NV-5138 is
265 capable of activating mTORC1, it cannot be utilized for protein synthesis.[45,46] To maximize
266 mTORC1 stimulation *ex vivo*, cells were cultured in leucine-free medium. Like *TSC2*
267 knockdown, NV-5138 stimulated mTORC1 and heightened amyloid levels in MPNST cells
268 (Figures S5M and 5E); however, it only elicited pronounced cytotoxicity with concurrent HSF1
269 inhibition (Figure 5F). Again, CR treatment largely blocked this cytotoxicity (Figure 5F). In
270 sharp contrast, combined NV-5138 and DTHIB treatment did not significantly impact non-
271 transformed Schwann cells (Figure 5G). Of interest, their mTORC1 signaling was less
272 responsive to NV-5138 stimulation (Figures S5N). We next reasoned that by directly
273 contributing to protein quantity, L-leucine might impact the cancer proteome more profoundly.
274 In both S462 and 90-8TL cells, L-leucine synergized with DTHIB to induce severe cytotoxicity

275 (Figures 5H and S5O). On the contrary, no cytotoxicity was induced in non-transformed
276 Schwann cells (Figure 5I).
277
278 To further corroborate the HSF1-dependent effects of DTHIB, we evaluated another direct
279 small-molecule HSF1 inhibitor KRIBB11[48], which blocks the recruitment of pTEFb likely
280 through binding to the transactivation domain of HSF1. KRIBB11, like DTHIB, synergized with
281 L-leucine to induce amyloids and trigger severe cytotoxicity in MPNST cells; importantly, CR
282 treatment both diminished amyloids and blocked cell death (Figures 5J and 5K).
283
284 Furthermore, in S462 cells shRNA-mediated *HSF1* knockdown and L-leucine stimulation
285 synergistically provoked prominent cytotoxicity as well (Figure 5L), providing a genetic
286 validation. Thus, these findings collectively indicate that mTORC1 stimulation synergizes with
287 HSF1 inhibition to rapidly trigger severe cytotoxicity in cancerous cells, in part by prompting
288 unconstrained proteomic imbalance and amyloidogenesis.
289
290 **Unconstrained proteomic imbalance incites non-apoptotic, non-autophagic death**
291 HSF1 inhibition alone induced both apoptotic and non-apoptotic death in MPNST cells,
292 distinguished by caspase 3 cleavage; intriguingly, concurrent mTORC1 stimulation caused a
293 striking shift towards non-apoptotic cell death, characterized by cell membrane permeabilization
294 without caspase 3 cleavage (Figures 6A and 6B).
295
296 To date, several modes of non-apoptotic cell death have been described, including pyroptosis,
297 necroptosis, ferroptosis, and autophagic death, all of which could result in loss of cell membrane

298 integrity. Corroborating a non-apoptotic mechanism, the pan-caspase inhibitor Q-VD-OPh did
299 not prevent the membrane permeabilization in *TSC2*-deficient MPNST cells treated with DTHIB
300 (Figures 6A and 6B).[49] However, it did block the apoptosis in control MPNST cells treated with
301 DTHIB (Figures 6A and S6A). As Q-VD-OPh inhibits caspase 1 and no caspase 1 cleavage was
302 detected (Figure S6B),[50] a key driver of pyroptosis,[51] this result does not support a pyroptotic cell
303 death either. Similarly, HSF1 inhibition did not induce necroptosis in *TSC2*-deficient MPNST
304 cells, evidenced by the lack of MLKL Ser358 phosphorylation (Figure S6B), an essential event
305 executing necroptosis.[52] Congruently, the necroptosis inhibitor necrostatin-1 exerted no effects
306 on the cell membrane disruption (Figures 6C and S6C).[52]
307
308 Intriguingly, HSF1 inhibition diminished glutathione peroxidase 4 (GPX4) but increased
309 transferrin receptor 1 (TFR1), which was accompanied with markedly elevated lipid
310 peroxidation, in *TSC2*-deficient MPNST cells (Figures 6D and S6D). All these changes are
311 indicative of ferroptosis.[53,54] Although in *TSC2*-deficient cells liproxstatin-1, a potent ferroptosis
312 inhibitor,[53,54] reversed the elevation of TFR1 elicited by the ferroptosis inducer erastin, it neither
313 blocked the marked increase in TFR1 nor stopped the membrane disruption induced by DTHIB
314 (Figures 6C, 6D, and S6C). This is not due to the defectiveness of necrostatin-1 and liproxstatin-
315 1, as both inhibitors potently blocked necroptosis and ferroptosis induced in HT-29 cells,
316 respectively (Figure S6E). HSF1 inhibition also elicited autophagy, evidenced by diminished
317 p62/SQSTM1 and elevated LC3B-II (Figure 6E).[55] To determine whether autophagic cell death
318 was implicated, we employed the class III PI3K inhibitor wortmannin to block autophagy.[56] As
319 expected, wortmannin effectively prevented the decreases in p62/SQSTM1 and LC3B-II induced
320 by rapamycin in *TSC2*-deficient MPNST cells (Figure 6E), indicating successful blockade of

321 autophagy. Nevertheless, wortmannin failed to block the cell membrane disruption in *TSC2*-
322 deficient cells treated with HSF1 inhibitors (Figures 6F and S6F). These findings suggest that
323 both ferroptosis and autophagy are the consequences, rather than the causes, of cell membrane
324 disruption. Collectively, our findings support that uncontained proteomic instability and ensuing
325 amyloidogenesis potently trigger cell death, which is neither apoptotic nor autophagic (Figure
326 6G). Moreover, several common modes of programmed necrosis are not deeply implicated as
327 well. The precise nature of this proteomic catastrophe-induced death (PCID), nonetheless,
328 remains to be fully delineated.
329
330 **Unconstrained proteomic imbalance suppresses *in vivo* tumor growth**
331 Due to the limited *in vivo* bioavailability of DTHIB in our mouse models, we focused on
332 KRIBB11 for *in vivo* studies. Consistent with *ex vivo* findings, combined L-leucine stimulation
333 and KRIBB11 administration significantly impaired the *in vivo* growth of xenografted human
334 S462 MPNST cells in immunocompromised mice (Figure 7A). Despite this overall impact, 2 out
335 of 8 tumors did not respond to the combination treatment (Figure S7A), creating large variations
336 and right-skewed distribution. Of note, without leucine stimulation KRIBB11 only marginally
337 affected tumor growth; by contrast, in the presence of leucine KRIBB11 did evidently slow
338 tumor exponential growth rates and delay tumor volume doubling time (Figures S7B). In
339 addition, mice receiving this combination treatment tended to survive better as well (Figure
340 S7C).
341
342 Next, we asked if this therapeutic strategy could be applied broadly. To this end, we established
343 a syngeneic mouse xenograft model of melanoma, where the murine melanoma B16-F10 cells

344 were transplanted into C57BL/6J mice. Like in the MPNST model, KRIBB11 combined with L-
345 leucine stimulation also impeded the tumor growth in this fast-growing tumor model (Figures 7B
346 and S7D). As expected, L-leucine stimulated mTORC1 signaling, evidenced by increased S6RP
347 phosphorylation (Figure 7C). KRIBB11 reduced the transcription of *Hspa1a/Hsp72* and
348 *Hspb1/Hsp25* in melanomas (Figure 7D), confirming a successful inhibition of HSF1.
349 Importantly, combined KRIBB11 administration and leucine stimulation markedly induced
350 amyloids in tumors (Figure 7E). By stark contrast, no amyloids were induced in normal tissues
351 including brains and spleens (Figures 7F and 7G). Treatments did not cause loss of body weights
352 in mice (Figure S7E). In aggregate, these *in vivo* findings from two distinct mouse models
353 support that unconstrained proteomic imbalance, provoked by combined HSF1 inhibition and
354 mTORC1 stimulation, causes proteomic catastrophe that is tumor suppressive (Figure 7H).
355
356
357
358
359
360
361
362
363
364
365
366

367 **DISCUSSIONS**

368 Genomic instability has been broadly recognized as a driver of oncogenesis. Contrastingly, the
369 implications of proteomic instability in cancer remain obscure.

370

371 **Proteomic instability is tumor suppressive but inevitable**

372 Proteomic instability does occur in cancer, evidenced by elevated protein polyubiquitination,
373 aggregation, and even amyloidogenesis. In cancer, proteomic instability can be ascribed to
374 several mechanisms, including protein oxidation by reactive oxygen species, protein misfolding
375 owing to genetic mutations, and augmentation of protein dosage caused by aneuploidy.[1,3]
376 Revealed by our recent studies, uncontrolled protein translation also contributes to
377 amyloidogenesis. This is not entirely surprising, as it has been estimated that up to 30% of all
378 newly synthesized polypeptides are misfolded and subjected to proteasomal degradation.[57]
379 Imaginably, aberrant protein synthesis would increase the chance of producing protein
380 aggregates and even amyloids, especially considering numerous genetic mutations affecting
381 protein folding in cancer cells. Dysregulated protein translation, ironically, is fundamental to
382 malignant growth, making proteomic instability and amyloidogenesis inevitable.

383

384 At the cellular level, amyloids are toxic to both neurons and cancer cells. At the organismal
385 level, amyloidogenesis is neurodegenerative but tumor suppressive. Mechanistically, our studies
386 demonstrate that soluble AOs can directly attack the guardian of the mitochondrial proteome
387 HSP60. Of course, mechanisms other than targeting HSP60 exist as well. Moreover, it remains to
388 be elucidated what other proteins comprise cancer-associated amyloids, in addition to the
389 Alzheimer's disease-associated Aβ.

390

391 **HSF1 contains proteomic instability to enable malignancy**

392 The multifaceted pro-oncogenic roles of HSF1 have been ascribed to a wide array of underlying
393 mechanisms; nonetheless, a universal one remains to be defined.

394

395 As an inevitable price of malignancy, proteomic instability must be contained by cancer cells to
396 avert tumor suppression and sustain malignant phenotypes. Now, our findings reveal that HSF1
397 contains proteomic instability, particularly amyloidogenesis, constituting a generic pro-
398 oncogenic mechanism. It is worth noting that HSF1 only contains and mitigates, but cannot
399 eradicate, amyloidogenesis, as uncontrolled protein translation is a direct cause of
400 amyloidogenesis in cancer cells. This dependency on HSF1 to contain proteomic instability
401 partly underlies the phenomenon of "HSF1 addiction of cancer".

402

403 Our studies further support that HSF1 contains amyloidogenesis via at least two mechanisms,
404 direct and indirect. On the one hand, through induction of HSPs, HSF1 ensures appropriate
405 protein folding to maintain a healthy proteome, thereby preventing the emergence of amyloids.
406 This is supported by the finding that HSF1 inhibition heightens protein ubiquitination,
407 aggregation, and amyloidogenesis. On the other hand, HSF1 can neutralize soluble AOs directly
408 once they emerge. Under this context, HSF1 inhibition would unleash AOs to assault HSP60,
409 inflicting mitochondrial damage and toxicity. Thus, in cancer cells HSF1 inhibition both enlarges
410 the quantity of amyloids and, more importantly, renders them toxic.

411

412 **mTORC1 signaling becomes tumor suppressive in the absence of HSF1**

413 Given the dependency of malignant growth on protein translation, unsurprisingly, mTORC1
414 signaling is hyperactive in human cancers, which is, canonically, considered oncogenic.[58,59]
415 Unexpectedly, our current studies reveal that mTORC1 signaling becomes tumor suppressive in
416 the absence of HSF1, owing to profound disproportion between protein quantity and quality.
417 This unconstrained proteomic imbalance, in turn, exacerbates proteomic instability and tumor-
418 suppressive amyloidogenesis. The notable blockage of cytotoxicity by either translation
419 inhibitors or CR lends strong support to this model. Conceptually, HSF1 empowers the
420 oncogenic potential of mTORC1 signaling, reinforcing HSF1 as an oncogenic enabler.
421
422 **Provoking proteomic catastrophe exemplifies a next-generation therapeutic concept**
423 Currently popular chemo-and radiotherapies mainly target the cancer genome, causing DNA
424 damage. An emerging horizon in cancer therapy is targeting the cancer proteome. To date, much
425 effort has been devoted to inhibiting individual HSP families, such as HSP70 and HSP90.[60,61]
426 However, every cell is equipped with both constitutive and inducible HSPs. While the former
427 constitute the basal chaperoning capacity that is essential to life, the latter supply the extra
428 chaperoning capacity, which is dispensable for normal life but required under stressful
429 conditions. Their structural and functional resemblances pose the biggest challenge for small
430 molecules to distinguish these cognate HSPs. Moreover, multiple families of HSPs, including
431 HSP100, HSP90, HSP70, HSP60, HSP40, and small HSPs, exist inside cells. Targeting single
432 HSP family would have limited therapeutic effects. Thus, new approaches or directions are
433 warranted to overcome these drawbacks.
434

435 Our and others' studies collectively support that malignant cells constantly endure intrinsic
436 proteotoxic stress, rendering HSF1 constitutively active. In turn, cancer cells become reliant on
437 the extra chaperoning capacity, conferred by HSF1, for their growth and survival. Thus, only
438 eliminating this extra chaperoning capacity but sparing the basal one would be an ideal strategy
439 to combat malignancy. Together, these concepts provide strong rationales for targeting HSF1 in
440 cancer. It is exciting to witness the recent launch of HSF1 inhibitors into clinical trials.[62]
441
442 In reaction to HSF1 inhibition, unsurprisingly, cancer cells attenuate their protein synthesis. This
443 adaptive response underscores the importance of balanced protein quantity and quality to cellular
444 fitness, a key concept inspiring us to explore driving proteomic imbalance for cancer therapy. Of
445 note, breaking this adaptation may impede tumor evolution.
446
447 The widespread hyperactivation of mTORC1 in human cancers makes it an attractive therapeutic
448 target. Hence, an array of mTOR inhibitors have been developed, several of which are actively
449 under clinical evaluation.[59,63] Thus far, these inhibitors have displayed mostly cytostatic effects
450 and less than expected therapeutic efficacies.[63,64] Considering the essentiality of protein
451 translation to life, profound mTORC1 inhibition would inflict undesirable toxicities in normal
452 cells and tissues. In fact, mTORC1 inhibitors have long been known as immunosuppressants.[63,65]
453
454 Opposite to the prevailing tactic in cancer therapy, we stimulated mTORC1 to drive proteomic
455 imbalance. Counterintuitive mTORC1 stimulation, when combined with HSF1 inhibition,
456 engendered catastrophic proteomic instability in cancer and elicited tumor suppression (Figure
457 7G). This PCID offers a wide therapeutic window, largely due to the lack of proteomic

instability and amyloidogenesis in primary cells and tissues. Conceivably, mTORC1 stimulation boosts production of wild-type proteins in primary cells, which can be easily managed without impacting well-preserved proteomic stability; in sharp contrast, it creates an enormous problem for the already stressed, fragile cancer proteome through synthesis of copious mutant, misfolded proteins. The adaptive response, noteworthily, still arises from concurrent mTORC1 stimulation and HSF1 inhibition in cancer. It is expected that additional, specific blockade of the JNK-mediated mTORC1 repression would further exacerbate proteomic imbalance, impelling cancerous cells to extinction. It remains possible that leucine stimulation could exert further mTORC1-independent effects, contributing to tumor suppression. Transcription factors, traditionally, have been regarded as "undruggable" targets for small molecules. While both DTHIB and KRIBB11 epitomize the prototypes of direct HSF1 inhibitors, their inadequate *in vivo* bioactivities render them unsuitable for clinical applications at the current state. Nevertheless, we herein accomplished the proof-of-concept experiments to demonstrate the feasibility of propelling proteomic catastrophe in cancer. This next-generation therapeutic concept may be applicable to a broad spectrum of human cancers and, with the advent of clinic-relevant molecules, holds promise for combating malignancy.

ACKNOWLEDGMENTS

We would like to thank the Optical Microscopy and Image Analysis lab (OMAL) for their assistance with the confocal microscopy studies and Holly Morris for her assistance in animal studies. Schematic illustrations are created with BioRender.com. This work was supported by the grant from Department of Defense Congressionally Directed Medical Research Programs to C.D. (NF150028) and by the Intramural Research Program of the NIH, National Cancer Institute, Center for Cancer Research (1ZIABC011767). The content of this publication does not necessarily reflect the views or policies of the Department of Health and Human Services, nor does mention of trade names, commercial products, or organizations imply endorsement by the U.S. government.

AUTHOR CONTRIBUTIONS: B.M.R., O. S., and K-H.C. designed and conducted the experiments. C.D. conceptualized and supervised this study and analyzed the results. B.M.R. and C.D. wrote the manuscript.

DECLARATION OF INTERESTS: The authors declare no competing interests.

504 **EXPERIMENTAL MATERIALS AND METHODS**

505 **Cells, Chemicals, and reagents**

506 S462 (female) and 90-8TL (female) cells were kindly provided by Dr. Karen Cichowski.
507 sNF96.2 cells (male) and immortalized human Schwann cells (hTERT ipn02.3 2λ, female) were
508 purchased from ATCC. Primary human Schwann cells (Cat#1700, ScienCell Research
509 Laboratories) were grown on poly-L-lysine coated T-75 flasks and maintained in complete
510 Schwann Cell Medium (Cat#1701, ScienCell Research Laboratories). B16-F10-luc2 (male)
511 cells were purchased from ATCC (cat#CRL-6475-LUC2). All cell lines, except 90-8TL and
512 HSCs (no known STR profiles available), were authenticated by ATCC. All cell lines, except
513 primary human Schwann cells, were maintained in DMEM supplemented with 10% HyClone
514 bovine growth serum and 1% penicillin–streptomycin. Cells were maintained in an incubator
515 with 5% CO2 at 37 °C.

516

517 The following chemicals were purchased from commercial sources: JNK-IN-8 (Cat#S4901,
518 Selleckchem), 6-FAM-dC-puromycin (cat#NU-925-6FM, Jena Bioscience), Congo red
519 (cat#B2431014, Thermo Scientific Chemicals), Thioflavin T (cat#211760050, Thermo Scientific
520 Chemicals), LY2584702 (cat#S7698, Selleckchem), 4EGI-1 (cat#S7369, Selleckchem), and
521 DTHIB (cat# HY-138280, MedChemExpress), KRIBB11 (cat#HY-100872, MedChemExpress),
522 KRIBB11 (cat#T3652, TargetMol Chemicals), Q-VD-OPh (cat#HY-12305, MedChemExpress),
523 necrostatin-1 (cat#HY-15760, MedChemExpress), Liproxstatin-1 (cat#HY-12726,
524 MedChemExpress), wortmannin (cat#HY-10197, MedChemExpress), rapamycin (cat#HY-
525 10219, MedChemExpress), erastin (cat#HY-15763, MedChemExpress), MHY1485 (cat#HY-
526 B0795, MedChemExpress), NV-5138 HCl (cat#HY-114384B, MedChemExpress), and Liperfluo

527 (cat#L248, Dojindo Laboratories), dimethylacetamide (cat#T19439, TargetMol Chemicals
528 Inc.), PEG300 (cat#T7022, TargetMol Chemicals Inc.), and Captisol (cat#RC-0C7-100, CyDex
529 Pharmaceuticals).
530
531 Rabbit phospho-4EBP1 S65/T70 antibody (cat#sc-12884-R), mouse monoclonal HSF1 (E-4,
532 cat#sc-17757) antibody, rabbit HSF1 antibody (H-311, cat#sc-9144), mouse monoclonal JNK
533 (D-2, cat#sc-7345), rabbit JNK1/3 (C-17, cat#sc-474) antibody were purchased from Santa
534 Cruz Biotechnology; antibodies for phosphor-4EBP1 Thr70 (cat#9455), phospho-4EBP1
535 Thr37/46 (236B4, cat#2855), phospho-p70S6K T389 (108D2, cat# 9234), phosphor-S6RP
536 Ser235/236 (D57.2.2E, cat#4858), p70 S6K (49D7, cat#2708), 4EBP1 (53H11, cat#9644),
537 S6RP (5G10, cat#2217), mTOR (7C10, cat#2983), phospho-JNK1/2 T183/Y185 (81E11,
538 cat#4668), JNK2 (56G8, cat#9258), c-Jun (60A8, cat#9165), phospho-c-Jun Ser63 II
539 (cat#9261), PARP (cat#9542), Tuberin/TSC2 (D93F12, cat#4308), SQSTM1/p62 (D1Q5S,
540 cat#39749), cleaved caspase 3 (Asp175) (5A1E, cat#9664), caspase 1(D7F10, cat#3866),
541 gasdermin D (E9S1X, cat#39754), phosphor-MLKL Ser358 (D6H3V, cat#91689), GPX4
542 (E5Y8K, cat#59735), and transferrin receptor/CD71 (H68.4, cat#46222) antibody were
543 purchased from Cell Signaling Technologies; mouse β-actin antibody-HRP (Cat#A00730)
544 conjugates were from GenScript. Anti-K48-specific ubiquitin antibody (Apu2, cat#05-1307)
545 and mouse monoclonal anti-RAPTOR antibody (1H6.2, cat#05-1470) were purchased from
546 EMD Millipore. Mouse monoclonal anti-JNK1 (C-terminal region) antibody (cat#JM2671)
547 was purchased from ECM Biosciences. Anti-amyloid oligomers (A11, cat#SPC-506D) and
548 anti-amyloid fibrils (OC, cat#SPC-507D) antibodies were purchased from StressMarq
549 Biosciences Inc. Mouse monoclonal anti-HSP60 antibody (LK-1, cat#ADI-SPA-806) was

550 purchased from Enzo Life Sciences Inc. β-Actin (cat#GTX629630), GAPDH
551 (cat#GTX627408), α-tubulin (GT114, cat#GTX628802), and LC3B antibody
552 (cat#GTX127375) was purchased from GeneTex Inc.
553

554 **METHOD DETAILS**

555 **Lentiviral Particle Production and Transduction of lentiviral shRNAs**

556 Lentiviral pLKO.1 shRNA plasmids targeting human *HSF1* were described previously[10]:
557 TRCN0000007480 (hA6) and TRCN0000007483 (hA9). The sequence of control hairpins
558 targeting a scrambled sequence with no known homology to any human genes is 5′-
559 CCTAAGGTTAAGTCGCCCTCG-3′. The pLKO.1 shRNA plasmid targeting human *TSC2* was
560 a gift from Do-Hyung Kim (Cat#15478, Addgene). Lentiviral pLKO shRNA plasmids were
561 transiently co-transfected individually along with plasmids encoding ΔVPR and VSV-G into
562 HEK293T cells using TurboFect™ (Cat#R0531, Thermo Scientific). Viral supernatants were
563 collected after centrifugation at 1,000 rpm for 15 min. Viral transduction was achieved by
564 incubating target cells with viral supernatants containing 10μg/ml polybrene (Cat#TR-1003-G,
565 Millipore-Sigma) for 24h. For stable knockdown of *TSC2,* lentivirus particles were prepared using
566 pLKO shRNA plasmids targeting human *TSC2*. Scrambled shRNA was used for stable control
567 cells. After 4 days of transduction, cells were gradually selected using 1-4 μg/ml puromycin for 2
568 weeks.

569 **Soluble and Insoluble Protein Fractionation**

570 Equal numbers of cells were incubated with cold cell-lysis buffer (100 mM NaCl, 30 mM Tris-
571 HCl pH 7.6, 1% Triton X-100, 20 mM sodium fluoride, 1mM EDTA, 1mM sodium
572 orthovanadate, and 1x Halt™ protease inhibitor cocktail) on ice for 20 min. The crude lysates
573 were first centrifuged at 500xg for 5 min at 4°C. The supernatants from low-speed (500xg)
574 centrifugation were transferred to a new Eppendorf tube. The first pellets were resuspended in
575 DNA digestion solution (2 units DNase I, 1% Triton X-100, 10 mM Tris-HCl, 2.5 mM
576 MgCl2, 0.5 mM CaCl2, pH 7.6) for 30 min at RT. An equal volume of 1xPBS with 2% SDS
577 was then added to resuspend the first pellets for additional 30 min at RT. Following the
578 centrifugation at 17,000xg for 10 min at RT, the supernatants were removed. The supernatants
579 from low-speed centrifuge were added back to the second pellets, followed by centrifugation
580 at 17,000xg for 15 min at 4°C. The final supernatants and pellets from high-speed (17,000xg)
581 centrifugation were collected as detergent-soluble and -insoluble fractions, respectively.
582 Insoluble fractions were further sonicated in 1xPBS with 2% SDS at high intensity using a
583 Bioruptor® Sonication Device (Diagenode) for SDS-PAGE.

584 **ThT and CR Staining for Flow Cytometry**

585 After washing with 1xPBS, cells were fixed with 4% formaldehyde at RT for 10 min.
586 Following fixation and 1xPBS washing, cells were resuspended in 1 ml permeabilization
587 buffer (1xPBS with 0.5% Triton X-100 and 3 mM EDTA) and incubated on ice for 30 min.
588 Following washing with 1xPBS, Cells were stained with 10 μM ThT or CR dissolved in
589 1xPBS for 5 min. Cells were washed and resuspended in PBS and fluorescence signals were
590 measured by a FACSCalibur, LSRFortessa X-20 or LSR II flow cytometer (BD Biosciences).

591 **Amyloid Oligomer and Fibril Quantitation by Direct ELISA and Flow Cytometry**

592 To quantitate soluble amyloid prefibrillar oligomers, soluble cell lysates diluted in 1xPBS
593 from equal numbers of cells were coated on each well in a 96-well ELISA plate at 4°C
594 overnight followed by blocking (5% non-fat milk in TBS-0.05% Tween® 20) at RT for 1 hr.
595 Each well was incubated with 100 µl amyloid oligomer antibodies (A11, 1:1,000 diluted in
596 the blocking buffer) at RT for 2 hr. After washing with TBS-T, goat anti-rabbit secondary Ab
597 HRP conjugates (1:1,000 diluted in blocking buffer) were added to each well and incubated at
598 RT for 1 hr. Following washing, 100 µl 1-Step Ultra TMB-ELISA substrates (Cat#34029,
599 Thermo Scientific) were added to each well. After adding 100µl Stop solution, absorbance was
600 measured at 450 nm using a SpectraMax iD5 microplate reader (Molecular Devices).

601 To quantitate amyloid fibrils, detergent-insoluble fractions from equal numbers of cells were
602 extracted as described in Soluble and Insoluble Protein Fractionation. The final pellets were
603 collected as detergent-insoluble fractions and solubilized by sonication for 15 min in 1xPBS
604 with 2% SDS. Solubilized proteins diluted in 1xPBS were added to each well and incubated at
605 37°C without cover overnight to air dry the wells. The following steps were identical to the
606 oligomer detection except for the use of amyloid fibril antibodies (OC) as the primary Ab.

607 For amyloid oligomer and fibril quantification by flow cytometry, cells were collected by
608 trypsinization and fixed in 4% Formaldehyde at RT for 10 min. Following permeabilization using
609 0.3% Triton-X-100, samples were incubated with primary antibodies A11-FITC (1:100 in 5%
610 BSA, StressMarq Biosciences, cat# SPC-506D-FITC) or OC-PerCP (1:100 in 5% BSA,
611 StressMarq Biosciences, cat# SPC-507D-PCP) at RT for 3 hrs. The cells were washed with PBS
612 and analyzed using flow cytometry.

613
614

615 **Measurement of Cell Viability**

616 Cell viability was determined using the CellTiter-Blue® Cell Viability Assay (cat#G8080,
617 Promega). Cells were grown in 96 well plates (1×10^4 per well) for 24h. A 20µl CellTiter-Blue®
618 reagent was added to 100µl of media in each well. The plates were incubated for 2h at 37°C and
619 the fluorescence was recorded at 560/590 nm. The reagents were discarded, and the wells were
620 washed with PBS before adding fresh media. Similarly, subsequent readings were recorded at
621 24h intervals till 96h time point.

622

623 **Proximity Ligation Assay**

624 Cells were fixed with 4% formaldehyde in PBS for 15 min at RT. After blocking with 5% normal
625 goat serum in PBS with 0.3% Triton X-100, primary antibodies 1:100 diluted in blocking buffer
626 were incubated with fixed cells overnight at 4°C. Following washing with PLA wash Buffer A,
627 samples were incubated with 1:5 diluted Duolink® in Situ PLA Probe anti-rabbit Plus
628 (cat#DUO92002, Sigma-Aldrich) and anti-mouse Minus (cat#DUO92004, Sigma-Aldrich) at
629 37°C for 1 hr. Subsequently, ligation (30 minutes, 37°C), rolling circle amplification, and detection
630 (120 minutes, 37°C) were performed using the Duolink® In Situ Detection Reagents Red
631 (cat#DUO92008, Sigma-Aldrich). Nuclei were counterstained with Hoechst 33342. PLA
632 signals were documented by a Zeiss LSM780 confocal microscope (Carl Zeiss). For PLA flow
633 cytometry, an equal number of cells were collected in microcentrifuge tubes by trypsinization and
634 fixed with 4% formaldehyde in PBS for 10 min at RT. Subsequent PLA steps were followed as
635 described earlier. The PLA signals were quantified by a FACSCalibur flow cytometer (BD
636 Biosciences).

637

638 Mouse anti-JNK1 (JM2671) and rabbit anti-HSF1 (H-311) antibodies were used for JNK-HSF1
639 PLA. Rabbit anti-JNK1/3 (C-17) and mouse anti-RAPTOR (1H6.2) antibodies were used for
640 JNK-RAPTOR PLA. Rabbit anti-mTOR (7C10) and mouse anti-RAPTOR (1H6.2) antibodies
641 were used for mTOR-RAPTOR PLA. Mouse anti-HSF1 (E-4) and rabbit anti-AO (A11)
642 antibodies were used for HSF1-AO PLA. Rabbit anti-AO (A11) and mouse anti-HSP60 (LK1)
643 antibodies were used for AO-HSP60 PLA.

644 **Measurement of global protein translation**

645 Live cells were incubated with 100 nM 6-FAM-dC-puromycin in complete culture medium
646 for 30 min and analyzed by a FACSCalibur flow cytometer (BD Biosciences).

647

648 **Immunoblotting and Immunoprecipitation**

649 Whole-cell protein extracts were prepared in cold cell-lysis buffer (100 mM NaCl, 30 mM Tris-
650 HCl pH 7.6, 1% Triton X-100, 20 mM sodium fluoride, 1mM EDTA, 1mM sodium
651 orthovanadate, and 1x Halt™ protease inhibitor cocktail). Proteins were transferred to
652 nitrocellulose membranes. Following incubation with the blocking buffer (5% non-fat milk in 1x
653 TBS-T) for 1 hour at RT, membranes were incubated with primary antibodies (1:1,000 dilution in
654 the blocking buffer) overnight at 4 °C. After washing with 1xTBS-T for 3 times, membranes
655 were incubated with peroxidase-conjugated secondary antibodies (1: 3,000 diluted in the
656 blocking buffer) at RT for 1 hr. Signals were detected using SuperSignal™ West
657 chemiluminescent substrates. For normal Co-IP, proteins were extracted using a QSonica Q125
658 sonicator (total process time: 15S, pulse-on time: 5S, pulse-off time: 10S, output intensity: 30%)
659 in 1x sonication buffer (20 mM Tris, 20 mM NaCl, 1 mM EDTA, 20 mM β-glycerol-phosphate,

660 20 mM sodium fluoride, 4 mM sodium orthovanadate, and 1 mM DTT pH7.4, supplemented
661 with Halt protease inhibitor cocktail). Total 1 mg whole cell lysates were incubated with A11
662 antibodies at 4 °C overnight. Normal rabbit IgG were used as the negative controls. The primary
663 antibody was precipitated using Protein G magnetic beads. After washing with the lysis buffer
664 for 3 times, beads were boiled in 1x loading buffer for 5 min before loading on SDS-PAGE.
665 EasyBlocker (Cat#GTX425858, GeneTex) was used for blocking and anti-HSF1 (H-311)
666 primary antibody (cat#sc-9144, Santa Cruz Biotechnology) incubation (1:1,000, O/N at 4°C).
667 The blot was incubated with EasyBlot anti-Rabbit IgG HRP conjugated antibody
668 (cat#GTX221666-01, GeneTex) for 1 hour. Chemiluminescent signals were captured by an
669 iBright™ FL1000 imaging system (ThermoFisher Scientific).
670
671 **Live-Or-Dye™ Dead Cell Staining**
672 Cells were cultured in DMEM for 48 hours before being treated with inhibitors for the required
673 periods and collected by trypsinization. $1x10^6$ cells/ml cells were stained with Live-or-Dye™
674 fixable dead cell dyes (1:1,000 dilution, cat#32003, Biotium) at RT for 30 min, protected from
675 light. Stained cells were washed once with PBS and analyzed by flow cytometry. For co-staining
676 with cleaved caspase 3 antibody, stained cells were fixed with 4% formaldehyde (10 min, RT)
677 and permeabilized with 0.3% Triton-X-100 in PBS (10 min, RT). The cells were stained by
678 Cleaved Caspase 3 antibody (Asp175) (5A1E) (1:1,000, cat#9664, Cell Signaling Technology)
679 followed by goat anti-Rabbit IgG Alexa Fluor™ 488 conjugated (1:1,000, cat#A-11034,
680 ThermoFisher Scientific) secondary antibodies. The samples were analyzed by flow cytometry.

681 **Inhibitor treatments**

682 Treatments with DTHIB, Q-VD-OPh, Liproxstatin-1, Necrostatin-1, and Wortmannin were
683 done for 72 hours. For Congo Red and LY-2584702 treatments, cells were pretreated for 24h
684 followed by DTHIB for an additional 72h. For treatments with NV-5138, cells were pretreated
685 for 48 hours in a leucine-free DMEM (cat#226-024, Crystalgen) before adding DTHIB for an
686 additional 72 hours.

687

688 **Animal studies**

689 All animal experiments described here were approved by the institutional Animal Care and Use
690 Committee (ACUC) of the National Cancer Institute, Frederick. Experiments on all animals
691 were conducted following the recommendations of the Guide for the Care and Use of
692 Laboratory Animals (National Academies Press, 2011). Animals were housed and maintained
693 on a 12-hour light/12-hour dark cycle at temperatures between 20°C and 27°C and humidity
694 levels of 30% to 70%, with food and water *available ad libitum*.

695 To establish the MPNST xenograft model, $9x10^6$ S462 MPNST cells (female) suspended with 30
696 % Matrigel were subcutaneously implanted the right flanks of 8-week-old female NIH-III nude
697 mice (Charles River Laboratories). After 7 days, xenografted mice were assigned to 4 groups,
698 eight each group, by stratified randomization based on tumor sizes (between 72 and 199 mm^3).
699 Mice were treated with KRIBB11 (65mg/kg, i.p. injection daily, cat#HY-100872, Lot#317606,
700 Medchemexpress LLC) with and without 2% L-leucine dissolved in drinking water stored in
701 amber-colored bottles. KRIBB11 was freshly dissolved daily in the vehicle (final
702 concentration:10% dimethylacetamide, 50% PEG300, 20% Captisol, and 20% sterile saline).

703

704 To establish the syngeneic melanoma model, 2 × 10^6 B16-F10-luc2 cells (male) mixed with
705 Matrigel (1:1 ratio) in a 200μL volume were subcutaneously implanted into the right flanks of
706 8-week-old C57BL/6J male mice (The Jackson Laboratory). After 5 days, xenografted mice were
707 assigned to 4 groups, eight each group, by stratified randomization based on tumor sizes (between
708 75 and 284 mm^3). Mice were treated with KRIBB11 (65 mg/kg, i.p. injection daily, cat#T3652,
709 Lot#132988, TargetMol Chemicals Inc.) with and without 2% L-leucine dissolved in drinking
710 water stored in amber-colored bottles. KRIBB11 was freshly dissolved daily in the vehicle (final
711 concentration:10% dimethylacetamide, 50% PEG300, 16% Captisol, and 24% sterile saline).

712 To formulate the KRIBB11 solution, KRIBB11 was first dissolved in dimethylacetamide,
713 followed by addition of PEG300. Lastly, 40 or 50% Capitol dissolved in sterile saline was added.
714 Tumor sizes were measured using a caliper by an animal technician blind to the study. To
715 assess the compound's toxicity, the body weight of tumor-bearing animals was also recorded.
716 Tumor volumes were estimated using the formula [length (mm) × $width^2$ (mm^2)]/2.
717

718 **Quantification And Statistical Analysis**

719 Statistical analyses were performed using Prism GraphPad 10.0 (GraphPad Software). The
720 detailed statistical methods and sample sizes are provided in the figure legends. All results are
721 expressed as mean±SD, mean±SEM, or median and IQR. The statistical significance is defined
722 as: *$p<0.05$, **$p<0.01$; ***$p<0.001$; ****$p<0.0001$; n.s.: not significant. For *in vitro*
723 experiments, sample size required was not determined a priori. The experiments were not
724 randomized**.** For *in vivo* experiments, sample size required was determined by pilot experiments.
725

726 **REFERENCES**

727 1. Dai C, Dai S, Cao J. Proteotoxic stress of cancer: implication of the heat-shock response in
728 oncogenesis. J Cell Physiol. 2012;227(8):2982-7. doi: 10.1002/jcp.24017. PubMed PMID:
729 22105155; PMCID: PMC3431153.
730 2. Dai C. The heat-shock, or HSF1-mediated proteotoxic stress, response in cancer: from
731 proteomic stability to oncogenesis. Philos Trans R Soc Lond B Biol Sci. 2018;373(1738). doi:
732 10.1098/rstb.2016.0525. PubMed PMID: 29203710; PMCID: PMC5717525.
733 3. Guang MHZ, Kavanagh EL, Dunne LP, Dowling P, Zhang L, Lindsay S, Bazou D, Goh CY,
734 Hanley C, Bianchi G, Anderson KC, O'Gorman P, McCann A. Targeting Proteotoxic Stress in
735 Cancer: A Review of the Role that Protein Quality Control Pathways Play in Oncogenesis.
736 Cancers (Basel). 2019;11(1). Epub 20190109. doi: 10.3390/cancers11010066. PubMed
737 PMID: 30634515; PMCID: PMC6356294.
738 4. Wilson DM, 3rd, Cookson MR, Van Den Bosch L, Zetterberg H, Holtzman DM, Dewachter I.
739 Hallmarks of neurodegenerative diseases. Cell. 2023;186(4):693-714. doi:
740 10.1016/j.cell.2022.12.032. PubMed PMID: 36803602.
741 5. Tang Z, Dai S, He Y, Doty RA, Shultz LD, Sampson SB, Dai C. MEK guards proteome
742 stability and inhibits tumor-suppressive amyloidogenesis via HSF1. Cell. 2015;160(4):729-44.
743 doi: 10.1016/j.cell.2015.01.028. PubMed PMID: 25679764; PMCID: PMC4564124.
744 6. Li J, Labbadia J, Morimoto RI. Rethinking HSF1 in Stress, Development, and Organismal
745 Health. Trends Cell Biol. 2017;27(12):895-905. Epub 20170907. doi:
746 10.1016/j.tcb.2017.08.002. PubMed PMID: 28890254; PMCID: PMC5696061.
747 7. Anckar J, Sistonen L. Regulation of HSF1 function in the heat stress response: implications in
748 aging and disease. Annu Rev Biochem. 2011;80:1089-115. doi: 10.1146/annurev-biochem-

749 060809-095203. PubMed PMID: 21417720.

750 8. Gomez-Pastor R, Burchfiel ET, Thiele DJ. Regulation of heat shock transcription factors and
751 their roles in physiology and disease. Nat Rev Mol Cell Biol. 2018;19(1):4-19. Epub
752 20170830. doi: 10.1038/nrm.2017.73. PubMed PMID: 28852220; PMCID: PMC5794010.

753 9. Min JN, Huang L, Zimonjic DB, Moskophidis D, Mivechi NF. Selective suppression of
754 lymphomas by functional loss of Hsf1 in a p53-deficient mouse model for spontaneous
755 tumors. Oncogene. 2007;26(35):5086-97. Epub 20070219. doi: 10.1038/sj.onc.1210317.
756 PubMed PMID: 17310987.

757 10. Dai C, Whitesell L, Rogers AB, Lindquist S. Heat shock factor 1 is a powerful multifaceted
758 modifier of carcinogenesis. Cell. 2007;130(6):1005-18. doi: 10.1016/j.cell.2007.07.020.
759 PubMed PMID: 17889646; PMCID: PMC2586609.

760 11. Meng L, Gabai VL, Sherman MY. Heat-shock transcription factor HSF1 has a critical role in
761 human epidermal growth factor receptor-2-induced cellular transformation and
762 tumorigenesis. Oncogene. 2010;29(37):5204-13. Epub 20100712. doi:
763 10.1038/onc.2010.277. PubMed PMID: 20622894; PMCID: PMC2940982.

764 12. Jin X, Moskophidis D, Mivechi NF. Heat shock transcription factor 1 is a key determinant of
765 HCC development by regulating hepatic steatosis and metabolic syndrome. Cell Metab.
766 2011;14(1):91-103. doi: 10.1016/j.cmet.2011.03.025. PubMed PMID: 21723507; PMCID:
767 PMC3214631.

768 13. Dai C, Santagata S, Tang Z, Shi J, Cao J, Kwon H, Bronson RT, Whitesell L, Lindquist S.
769 Loss of tumor suppressor NF1 activates HSF1 to promote carcinogenesis. J Clin Invest.
770 2012;122(10):3742-54. Epub 20120904. doi: 10.1172/JCI62727. PubMed PMID: 22945628;
771 PMCID: PMC3461912.

772 14. Kourtis N, Lazaris C, Hockemeyer K, Balandran JC, Jimenez AR, Mullenders J, Gong Y,
773 Trimarchi T, Bhatt K, Hu H, Shrestha L, Ambesi-Impiombato A, Kelliher M, Paietta E,
774 Chiosis G, Guzman ML, Ferrando AA, Tsirigos A, Aifantis I. Oncogenic hijacking of the
775 stress response machinery in T cell acute lymphoblastic leukemia. Nat Med.
776 2018;24(8):1157-66. Epub 20180723. doi: 10.1038/s41591-018-0105-8. PubMed PMID:
777 30038221; PMCID: PMC6082694.
778 15. Fujimoto M, Takii R, Matsumoto M, Okada M, Nakayama KI, Nakato R, Fujiki K, Shirahige
779 K, Nakai A. HSF1 phosphorylation establishes an active chromatin state via the TRRAP-
780 TIP60 complex and promotes tumorigenesis. Nat Commun. 2022;13(1):4355. Epub
781 20220729. doi: 10.1038/s41467-022-32034-4. PubMed PMID: 35906200; PMCID:
782 PMC9338313.
783 16. Heimberger T, Andrulis M, Riedel S, Stuhmer T, Schraud H, Beilhack A, Bumm T, Bogen
784 B, Einsele H, Bargou RC, Chatterjee M. The heat shock transcription factor 1 as a potential
785 new therapeutic target in multiple myeloma. Br J Haematol. 2013;160(4):465-76. Epub
786 20121218. doi: 10.1111/bjh.12164. PubMed PMID: 23252346.
787 17. Chuma M, Sakamoto N, Nakai A, Hige S, Nakanishi M, Natsuizaka M, Suda G, Sho T,
788 Hatanaka K, Matsuno Y, Yokoo H, Kamiyama T, Taketomi A, Fujii G, Tashiro K, Hikiba Y,
789 Fujimoto M, Asaka M, Maeda S. Heat shock factor 1 accelerates hepatocellular carcinoma
790 development by activating nuclear factor-kappaB/mitogen-activated protein kinase.
791 Carcinogenesis. 2014;35(2):272-81. Epub 20131015. doi: 10.1093/carcin/bgt343. PubMed
792 PMID: 24130164.
793 18. Fujimoto M, Takaki E, Takii R, Tan K, Prakasam R, Hayashida N, Iemura S, Natsume T,
794 Nakai A. RPA assists HSF1 access to nucleosomal DNA by recruiting histone chaperone

795 FACT. Mol Cell. 2012;48(2):182-94. Epub 20120830. doi: 10.1016/j.molcel.2012.07.026.
796 PubMed PMID: 22940245.
797 19. Solimini NL, Luo J, Elledge SJ. Non-oncogene addiction and the stress phenotype of cancer
798 cells. Cell. 2007;130(6):986-8. doi: 10.1016/j.cell.2007.09.007. PubMed PMID: 17889643.
799 20. Gutmann DH, Ferner RE, Listernick RH, Korf BR, Wolters PL, Johnson KJ.
800 Neurofibromatosis type 1. Nat Rev Dis Primers. 2017;3:17004. Epub 20170223. doi:
801 10.1038/nrdp.2017.4. PubMed PMID: 28230061.
802 21. Hirbe AC, Gutmann DH. Neurofibromatosis type 1: a multidisciplinary approach to care.
803 Lancet Neurol. 2014;13(8):834-43. doi: 10.1016/S1474-4422(14)70063-8. PubMed PMID:
804 25030515.
805 22. Cichowski K, Jacks T. NF1 tumor suppressor gene function: narrowing the GAP. Cell.
806 2001;104(4):593-604. doi: 10.1016/s0092-8674(01)00245-8. PubMed PMID: 11239415.
807 23. Grice GL, Nathan JA. The recognition of ubiquitinated proteins by the proteasome. Cell Mol
808 Life Sci. 2016;73(18):3497-506. Epub 20160502. doi: 10.1007/s00018-016-2255-5. PubMed
809 PMID: 27137187; PMCID: PMC4980412.
810 24. Knowles TP, Vendruscolo M, Dobson CM. The amyloid state and its association with protein
811 misfolding diseases. Nat Rev Mol Cell Biol. 2014;15(6):384-96. doi: 10.1038/nrm3810.
812 PubMed PMID: 24854788.
813 25. Yakupova EI, Bobyleva LG, Vikhlyantsev IM, Bobylev AG. Congo Red and amyloids:
814 history and relationship. Biosci Rep. 2019;39(1). Epub 20190115. doi:
815 10.1042/BSR20181415. PubMed PMID: 30567726; PMCID: PMC6331669.
816 26. Kayed R, Head E, Thompson JL, McIntire TM, Milton SC, Cotman CW, Glabe CG.
817 Common structure of soluble amyloid oligomers implies common mechanism of

818 pathogenesis. Science. 2003;300(5618):486-9. doi: 10.1126/science.1079469. PubMed
819 PMID: 12702875.
820 27. Kayed R, Head E, Sarsoza F, Saing T, Cotman CW, Necula M, Margol L, Wu J, Breydo L,
821 Thompson JL, Rasool S, Gurlo T, Butler P, Glabe CG. Fibril specific, conformation
822 dependent antibodies recognize a generic epitope common to amyloid fibrils and fibrillar
823 oligomers that is absent in prefibrillar oligomers. Mol Neurodegener. 2007;2:18. Epub
824 20070926. doi: 10.1186/1750-1326-2-18. PubMed PMID: 17897471; PMCID:
825 PMC2100048.
826 28. Heiser V, Scherzinger E, Boeddrich A, Nordhoff E, Lurz R, Schugardt N, Lehrach H,
827 Wanker EE. Inhibition of huntingtin fibrillogenesis by specific antibodies and small
828 molecules: implications for Huntington's disease therapy. Proc Natl Acad Sci U S A.
829 2000;97(12):6739-44. doi: 10.1073/pnas.110138997. PubMed PMID: 10829068; PMCID:
830 PMC18723.
831 29. Sanchez I, Mahlke C, Yuan J. Pivotal role of oligomerization in expanded polyglutamine
832 neurodegenerative disorders. Nature. 2003;421(6921):373-9. doi: 10.1038/nature01301.
833 PubMed PMID: 12540902.
834 30. Tang Z, Su KH, Xu M, Dai C. HSF1 physically neutralizes amyloid oligomers to empower
835 overgrowth and bestow neuroprotection. Sci Adv. 2020;6(46). Epub 20201111. doi:
836 10.1126/sciadv.abc6871. PubMed PMID: 33177089; PMCID: PMC7673739.
837 31. Christensen JH, Nielsen MN, Hansen J, Fuchtbauer A, Fuchtbauer EM, West M, Corydon
838 TJ, Gregersen N, Bross P. Inactivation of the hereditary spastic paraplegia-associated Hspd1
839 gene encoding the Hsp60 chaperone results in early embryonic lethality in mice. Cell Stress
840 Chaperones. 2010;15(6):851-63. doi: 10.1007/s12192-010-0194-x. PubMed PMID:

841 20393889; PMCID: PMC3024079.
842 32. Fan F, Duan Y, Yang F, Trexler C, Wang H, Huang L, Li Y, Tang H, Wang G, Fang X, Liu
843 J, Jia N, Chen J, Ouyang K. Deletion of heat shock protein 60 in adult mouse cardiomyocytes
844 perturbs mitochondrial protein homeostasis and causes heart failure. Cell Death Differ.
845 2020;27(2):587-600. Epub 20190617. doi: 10.1038/s41418-019-0374-x. PubMed PMID:
846 31209364; PMCID: PMC7205885.
847 33. Su KH, Cao J, Tang Z, Dai S, He Y, Sampson SB, Benjamin IJ, Dai C. HSF1 critically
848 attunes proteotoxic stress sensing by mTORC1 to combat stress and promote growth. Nat
849 Cell Biol. 2016;18(5):527-39. Epub 20160404. doi: 10.1038/ncb3335. PubMed PMID:
850 27043084; PMCID: PMC5341796.
851 34. Johnson GL, Nakamura K. The c-jun kinase/stress-activated pathway: regulation, function
852 and role in human disease. Biochim Biophys Acta. 2007;1773(8):1341-8. Epub 20070104.
853 doi: 10.1016/j.bbamcr.2006.12.009. PubMed PMID: 17306896; PMCID: PMC1995559.
854 35. Battaglioni S, Benjamin D, Walchli M, Maier T, Hall MN. mTOR substrate phosphorylation
855 in growth control. Cell. 2022;185(11):1814-36. Epub 20220516. doi:
856 10.1016/j.cell.2022.04.013. PubMed PMID: 35580586.
857 36. Kim DH, Sarbassov DD, Ali SM, King JE, Latek RR, Erdjument-Bromage H, Tempst P,
858 Sabatini DM. mTOR interacts with raptor to form a nutrient-sensitive complex that signals to
859 the cell growth machinery. Cell. 2002;110(2):163-75. doi: 10.1016/s0092-8674(02)00808-5.
860 PubMed PMID: 12150925.
861 37. Schmidt EK, Clavarino G, Ceppi M, Pierre P. SUnSET, a nonradioactive method to monitor
862 protein synthesis. Nat Methods. 2009;6(4):275-7. Epub 20090322. doi: 10.1038/nmeth.1314.
863 PubMed PMID: 19305406.

864 38. Zhang T, Inesta-Vaquera F, Niepel M, Zhang J, Ficarro SB, Machleidt T, Xie T, Marto JA,
865 Kim N, Sim T, Laughlin JD, Park H, LoGrasso PV, Patricelli M, Nomanbhoy TK, Sorger
866 PK, Alessi DR, Gray NS. Discovery of potent and selective covalent inhibitors of JNK.
867 Chem Biol. 2012;19(1):140-54. doi: 10.1016/j.chembiol.2011.11.010. PubMed PMID:
868 22284361; PMCID: PMC3270411.
869 39. Moerke NJ, Aktas H, Chen H, Cantel S, Reibarkh MY, Fahmy A, Gross JD, Degterev A,
870 Yuan J, Chorev M, Halperin JA, Wagner G. Small-molecule inhibition of the interaction
871 between the translation initiation factors eIF4E and eIF4G. Cell. 2007;128(2):257-67. doi:
872 10.1016/j.cell.2006.11.046. PubMed PMID: 17254965.
873 40. Tolcher A, Goldman J, Patnaik A, Papadopoulos KP, Westwood P, Kelly CS, Bumgardner
874 W, Sams L, Geeganage S, Wang T, Capen AR, Huang J, Joseph S, Miller J, Benhadji KA,
875 Brail LH, Rosen LS. A phase I trial of LY2584702 tosylate, a p70 S6 kinase inhibitor, in
876 patients with advanced solid tumours. Eur J Cancer. 2014;50(5):867-75. Epub 20140115.
877 doi: 10.1016/j.ejca.2013.11.039. PubMed PMID: 24440085.
878 41. Porter AG, Janicke RU. Emerging roles of caspase-3 in apoptosis. Cell Death Differ.
879 1999;6(2):99-104. doi: 10.1038/sj.cdd.4400476. PubMed PMID: 10200555.
880 42. Boulares AH, Yakovlev AG, Ivanova V, Stoica BA, Wang G, Iyer S, Smulson M. Role of
881 poly(ADP-ribose) polymerase (PARP) cleavage in apoptosis. Caspase 3-resistant PARP
882 mutant increases rates of apoptosis in transfected cells. J Biol Chem. 1999;274(33):22932-40.
883 doi: 10.1074/jbc.274.33.22932. PubMed PMID: 10438458.
884 43. Huang J, Manning BD. The TSC1-TSC2 complex: a molecular switchboard controlling cell
885 growth. Biochem J. 2008;412(2):179-90. doi: 10.1042/BJ20080281. PubMed PMID:
886 18466115; PMCID: PMC2735030.

887 44. Dong B, Jaeger AM, Hughes PF, Loiselle DR, Hauck JS, Fu Y, Haystead TA, Huang J,
888 Thiele DJ. Targeting therapy-resistant prostate cancer via a direct inhibitor of the human heat
889 shock transcription factor 1. Sci Transl Med. 2020;12(574). doi:
890 10.1126/scitranslmed.abb5647. PubMed PMID: 33328331; PMCID: PMC10571035.
891 45. Sengupta S, Giaime E, Narayan S, Hahm S, Howell J, O'Neill D, Vlasuk GP, Saiah E.
892 Discovery of NV-5138, the first selective Brain mTORC1 activator. Sci Rep.
893 2019;9(1):4107. Epub 20190311. doi: 10.1038/s41598-019-40693-5. PubMed PMID:
894 30858438; PMCID: PMC6412019.
895 46. Kato T, Pothula S, Liu RJ, Duman CH, Terwilliger R, Vlasuk GP, Saiah E, Hahm S, Duman
896 RS. Sestrin modulator NV-5138 produces rapid antidepressant effects via direct mTORC1
897 activation. J Clin Invest. 2019;129(6):2542-54. Epub 20190416. doi: 10.1172/JCI126859.
898 PubMed PMID: 30990795; PMCID: PMC6546461.
899 47. Wolfson RL, Chantranupong L, Saxton RA, Shen K, Scaria SM, Cantor JR, Sabatini DM.
900 Sestrin2 is a leucine sensor for the mTORC1 pathway. Science. 2016;351(6268):43-8. Epub
901 20151008. doi: 10.1126/science.aab2674. PubMed PMID: 26449471; PMCID:
902 PMC4698017.
903 48. Yoon YJ, Kim JA, Shin KD, Shin DS, Han YM, Lee YJ, Lee JS, Kwon BM, Han DC.
904 KRIBB11 inhibits HSP70 synthesis through inhibition of heat shock factor 1 function by
905 impairing the recruitment of positive transcription elongation factor b to the hsp70 promoter.
906 J Biol Chem. 2011;286(3):1737-47. Epub 20101115. doi: 10.1074/jbc.M110.179440.
907 PubMed PMID: 21078672; PMCID: PMC3023468.
908 49. Caserta TM, Smith AN, Gultice AD, Reedy MA, Brown TL. Q-VD-OPh, a broad spectrum
909 caspase inhibitor with potent antiapoptotic properties. Apoptosis. 2003;8(4):345-52. doi:

910 10.1023/a:1024116916932. PubMed PMID: 12815277.
911 50. Chauvier D, Ankri S, Charriaut-Marlangue C, Casimir R, Jacotot E. Broad-spectrum caspase
912 inhibitors: from myth to reality? Cell Death Differ. 2007;14(2):387-91. Epub 20060929. doi:
913 10.1038/sj.cdd.4402044. PubMed PMID: 17008913.
914 51. Miao EA, Rajan JV, Aderem A. Caspase-1-induced pyroptotic cell death. Immunol Rev.
915 2011;243(1):206-14. doi: 10.1111/j.1600-065X.2011.01044.x. PubMed PMID: 21884178;
916 PMCID: PMC3609431.
917 52. Shan B, Pan H, Najafov A, Yuan J. Necroptosis in development and diseases. Genes Dev.
918 2018;32(5-6):327-40. doi: 10.1101/gad.312561.118. PubMed PMID: 29593066; PMCID:
919 PMC5900707.
920 53. Chen X, Comish PB, Tang D, Kang R. Characteristics and Biomarkers of Ferroptosis. Front
921 Cell Dev Biol. 2021;9:637162. Epub 20210121. doi: 10.3389/fcell.2021.637162. PubMed
922 PMID: 33553189; PMCID: PMC7859349.
923 54. Stockwell BR. Ferroptosis turns 10: Emerging mechanisms, physiological functions, and
924 therapeutic applications. Cell. 2022;185(14):2401-21. doi: 10.1016/j.cell.2022.06.003.
925 PubMed PMID: 35803244; PMCID: PMC9273022.
926 55. Yoshii SR, Mizushima N. Monitoring and Measuring Autophagy. Int J Mol Sci. 2017;18(9).
927 Epub 20170828. doi: 10.3390/ijms18091865. PubMed PMID: 28846632; PMCID:
928 PMC5618514.
929 56. Blommaart EF, Krause U, Schellens JP, Vreeling-Sindelarova H, Meijer AJ. The
930 phosphatidylinositol 3-kinase inhibitors wortmannin and LY294002 inhibit autophagy in
931 isolated rat hepatocytes. Eur J Biochem. 1997;243(1-2):240-6. doi: 10.1111/j.1432-
932 1033.1997.0240a.x. PubMed PMID: 9030745.

933 57. Schubert U, Anton LC, Gibbs J, Norbury CC, Yewdell JW, Bennink JR. Rapid degradation
934 of a large fraction of newly synthesized proteins by proteasomes. Nature.
935 2000;404(6779):770-4. doi: 10.1038/35008096. PubMed PMID: 10783891.
936 58. Kim LC, Cook RS, Chen J. mTORC1 and mTORC2 in cancer and the tumor
937 microenvironment. Oncogene. 2017;36(16):2191-201. Epub 20161017. doi:
938 10.1038/onc.2016.363. PubMed PMID: 27748764; PMCID: PMC5393956.
939 59. Zou Z, Tao T, Li H, Zhu X. mTOR signaling pathway and mTOR inhibitors in cancer:
940 progress and challenges. Cell Biosci. 2020;10:31. Epub 20200310. doi: 10.1186/s13578-020-
941 00396-1. PubMed PMID: 32175074; PMCID: PMC7063815.
942 60. Goloudina AR, Demidov ON, Garrido C. Inhibition of HSP70: a challenging anti-cancer
943 strategy. Cancer Lett. 2012;325(2):117-24. Epub 20120628. doi:
944 10.1016/j.canlet.2012.06.003. PubMed PMID: 22750096.
945 61. Jhaveri K, Taldone T, Modi S, Chiosis G. Advances in the clinical development of heat
946 shock protein 90 (Hsp90) inhibitors in cancers. Biochim Biophys Acta. 2012;1823(3):742-
947 55. Epub 20111029. doi: 10.1016/j.bbamcr.2011.10.008. PubMed PMID: 22062686;
948 PMCID: PMC3288123.
949 62. Pasqua AE, Sharp SY, Chessum NEA, Hayes A, Pellegrino L, Tucker MJ, Miah A, Wilding
950 B, Evans LE, Rye CS, Mok NY, Liu M, Henley AT, Gowan S, De Billy E, Te Poele R,
951 Powers M, Eccles SA, Clarke PA, Raynaud FI, Workman P, Jones K, Cheeseman MD. HSF1
952 Pathway Inhibitor Clinical Candidate (CCT361814/NXP800) Developed from a Phenotypic
953 Screen as a Potential Treatment for Refractory Ovarian Cancer and Other Malignancies. J
954 Med Chem. 2023;66(8):5907-36. Epub 20230405. doi: 10.1021/acs.jmedchem.3c00156.
955 PubMed PMID: 37017629; PMCID: PMC10150365.

63. Ali ES, Mitra K, Akter S, Ramproshad S, Mondal B, Khan IN, Islam MT, Sharifi-Rad J, Calina D, Cho WC. Recent advances and limitations of mTOR inhibitors in the treatment of cancer. Cancer Cell Int. 2022;22(1):284. Epub 20220915. doi: 10.1186/s12935-022-02706-8. PubMed PMID: 36109789; PMCID: PMC9476305.

64. Wood KC, Gutkind JS. Challenges and Emerging Opportunities for Targeting mTOR in Cancer. Cancer Res. 2022;82(21):3884-7. doi: 10.1158/0008-5472.CAN-22-0602. PubMed PMID: 36321262; PMCID: PMC9634680.

65. Thomson AW, Turnquist HR, Raimondi G. Immunoregulatory functions of mTOR inhibition. Nat Rev Immunol. 2009;9(5):324-37. doi: 10.1038/nri2546. PubMed PMID: 19390566; PMCID: PMC2847476.

Figure 1

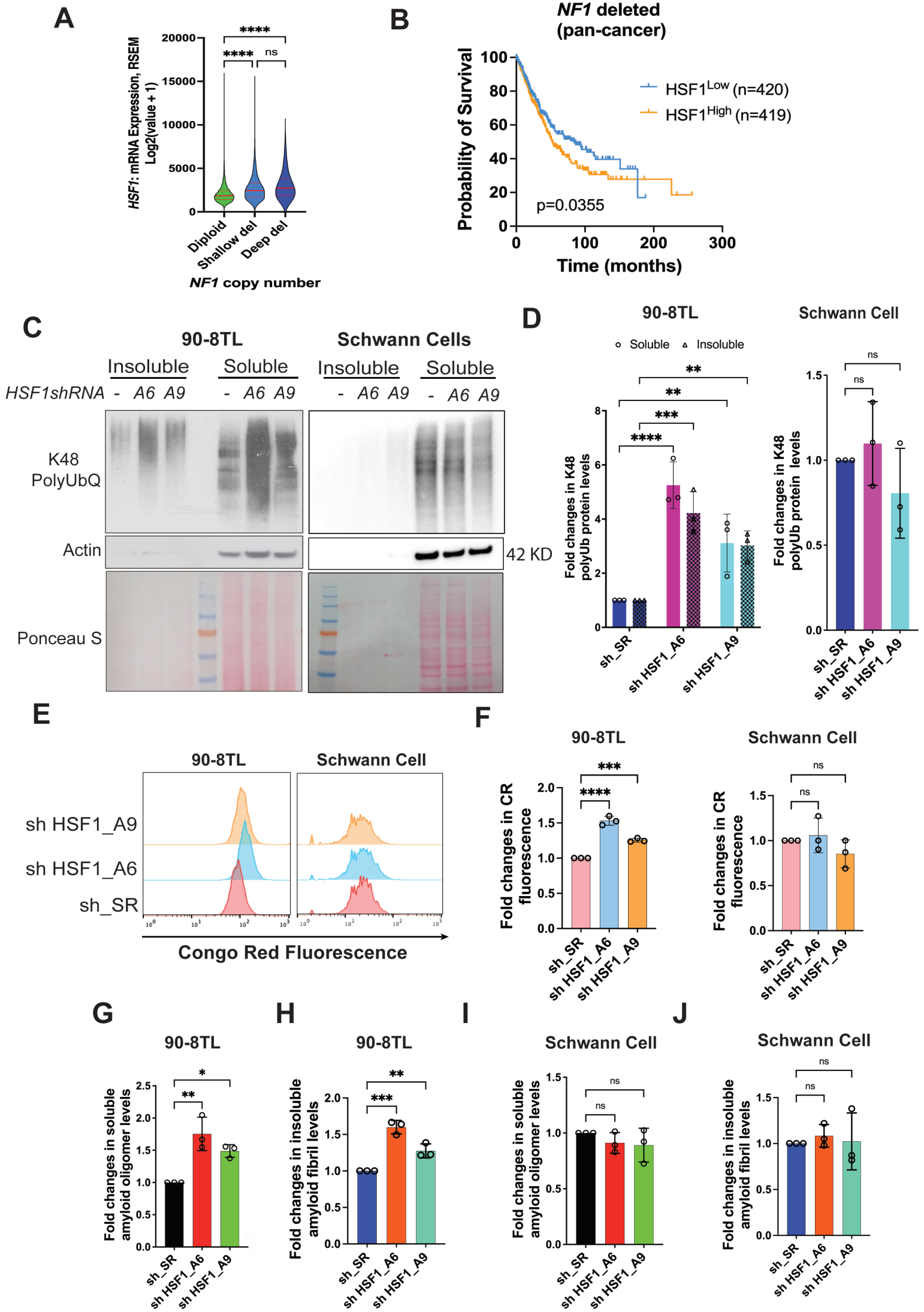
A
HSF1: mRNA Expression, RSEM Log2(value + 1)
20000
15000
10000
5000
0
****
****
ns
Diploid
Shallow del
Deep del
NF1 copy number
B
NF1 deleted (pan-cancer)
Probability of Survival
100
80
60
40
20
0
HSF1Low (n=420)
HSF1High (n=419)
p=0.0355
0
100
200
300
Time (months)
C
90-8TL
Schwann Cells
Insoluble
Soluble
Insoluble
Soluble
HSF1shRNA - A6 A9 - A6 A9 - A6 A9 - A6 A9
K48 PolyUbQ
Actin
42 KD
Ponceau S
D
90-8TL
Schwann Cell
Soluble
Insoluble
Fold changes in K48 polyUb protein levels
**
**
***
****
ns
ns
sh_SR
sh HSF1_A6
sh HSF1_A9
E
90-8TL
Schwann Cell
sh HSF1_A9
sh HSF1_A6
sh_SR
Congo Red Fluorescence
F
90-8TL
Schwann Cell
Fold changes in CR fluorescence
***
****
ns
ns
sh_SR
sh HSF1_A6
sh HSF1_A9
G
90-8TL
Fold changes in soluble amyloid oligomer levels
*
**
H
90-8TL
Fold changes in insoluble amyloid fibril levels
**
***
I
Schwann Cell
Fold changes in soluble amyloid oligomer levels
ns
ns
J
Schwann Cell
Fold changes in insoluble amyloid fibril levels
ns
ns

979 **FIGURE LEGENDS:**

980 **Figure 1: HSF1 is required to suppress proteomic instability and amyloidogenesis in**
981 **MPNST cells.** (A) Violin plots of *HSF1* expression in human cancer tissues showing *NF1*
982 deletion (median and IQR, n=6424, 1598, or 88, Kruskal-Wallis test). Data are generated by the
983 TGCA Research Network (https://www.cancer.gov/tcga). (B) Kaplan-Meier survival curves of
984 patients whose tumors harbor *NF1* deletion (n=420 or 419, Log-rank test). Data are generated by
985 the TGCA Research Network (https://www.cancer.gov/tcga). (C) and (D) The impacts of *HSF1*
986 depletion on protein polyubiquitination in both 90-8TL cells and primary human Schwann cells.
987 Cells were transduced with lentiviral shRNAs for 4 days and global protein Lys48-specific
988 ubiquitination was detected by immunoblotting in both detergent-soluble and -insoluble fractions
989 of whole cell lysates (C). Protein ubiquitination was quantitated using Fiji imaging software (D)
990 (mean ± SD, n=3 independent experiments, Two-way ANOVA). (E) and (F) Congo Red (CR)
991 staining of 90-8TL cells and primary human Schwann cells with and without *HSF1* depletion,
992 analyzed by flow cytometry (E). Quantitation of CR staining using the median fluorescence
993 intensity (F) (mean ± SD, n=3 independent experiments, One-way ANOVA). (G)-(J)
994 Quantitation of soluble amyloid oligomers and insoluble amyloid fibrils by ELISA using A11
995 and OC antibodies, respectively (mean ± SD, n=3 independent experiments, One-way ANOVA).
996
997
998
999
1000
1001

Figure 2

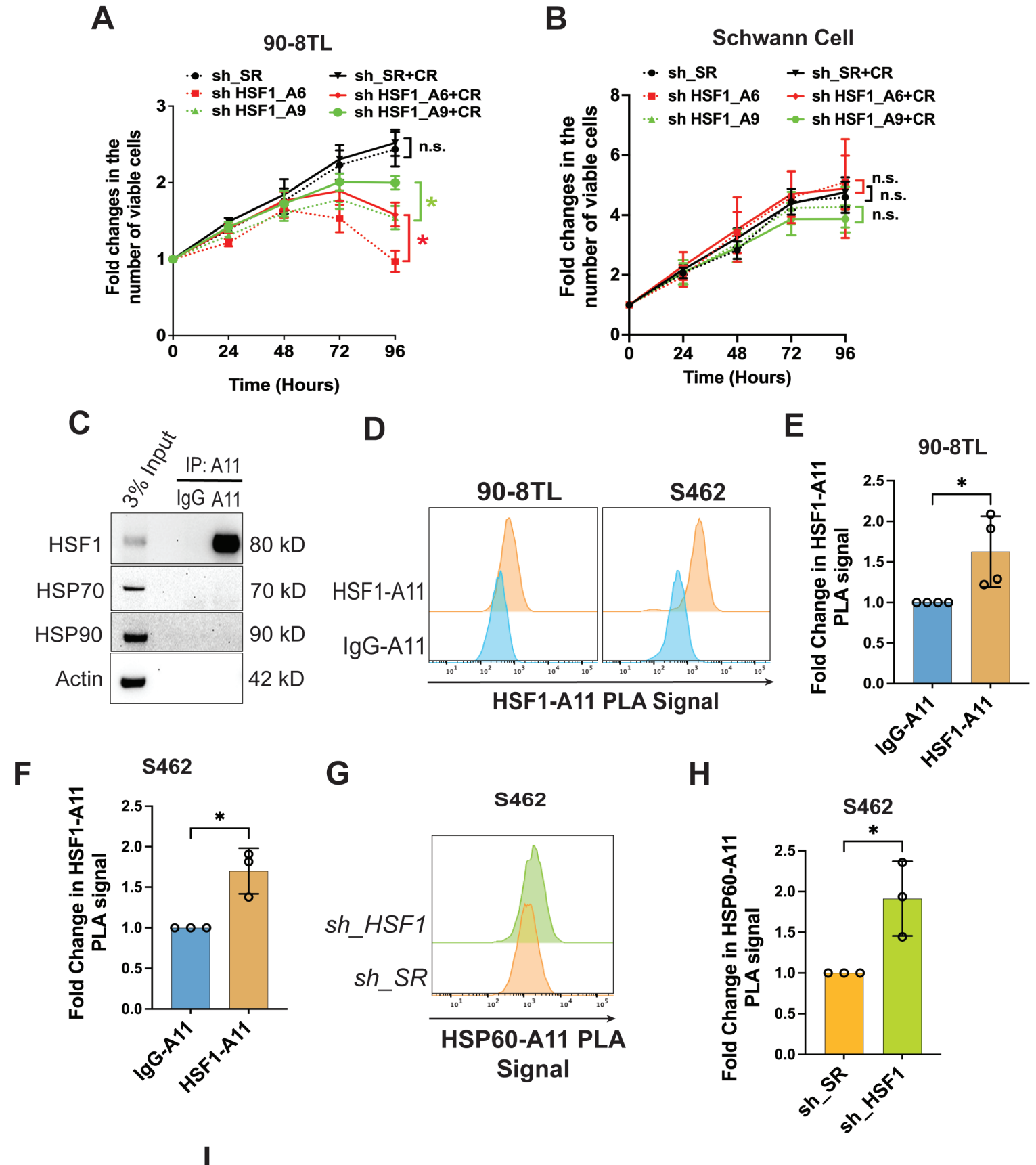
A
90-8TL
sh_SR
sh HSF1_A6
sh HSF1_A9
sh_SR+CR
sh HSF1_A6+CR
sh HSF1_A9+CR
Fold changes in the number of viable cells
Time (Hours)
n.s.
*
*
B
Schwann Cell
sh_SR
sh HSF1_A6
sh HSF1_A9
sh_SR+CR
sh HSF1_A6+CR
sh HSF1_A9+CR
Fold changes in the number of viable cells
Time (Hours)
n.s.
n.s.
n.s.
C
3% Input
IP: A11
IgG A11
HSF1
HSP70
HSP90
Actin
80 kD
70 kD
90 kD
42 kD
D
90-8TL
S462
HSF1-A11
IgG-A11
HSF1-A11 PLA Signal
E
90-8TL
Fold Change in HSF1-A11 PLA signal
*
IgG-A11
HSF1-A11
F
S462
Fold Change in HSF1-A11 PLA signal
*
IgG-A11
HSF1-A11
G
S462
sh_HSF1
sh_SR
HSP60-A11 PLA Signal
H
S462
Fold Change in HSP60-A11 PLA signal
*
sh_SR
sh_HSF1
I
Mitochondrial proteomic stability
Mitochondrial proteomic instability
HSF1
HSP60
AO

1002 **Figure 2: HSF1 counters the tumor-suppressive effects of amyloids in MPNST cells.**
1003 (A) and (B) The growth curves of 90-8TL and primary human Schwann cells with and without
1004 *HSF1* depletion and 20 μM CR treatment (mean ± SD, n=3 independent experiments, Two-way
1005 ANOVA). (C) Co-IP of amyloid oligomers (AOs) with HSF1 in 90-8TL cells. (D)-(F) Detection
1006 of AO–HSF1 interactions by PLA flow cytometry in 90-8TL and S462 cells. Quantitation of the
1007 PLA signals using the median fluorescence intensity (mean ± SD, n=3 or 4 independent
1008 experiments, Student's t test). (G) and (H) Detection of AO–HSP60 interactions by PLA flow
1009 cytometry in S462 cells following *HSF1* depletion (G). Quantitation of the PLA signals using the
1010 median fluorescence intensity (H) (mean ± SD, n=3 independent experiments, Student's t test).
1011 (I) Schematic depiction of AO neuralization by HSF1 and HSP60 attack by AO following *HSF1*
1012 depletion in mitochondria.
1013
1014
1015
1016
1017
1018
1019
1020
1021
1022
1023
1024

Figure 3

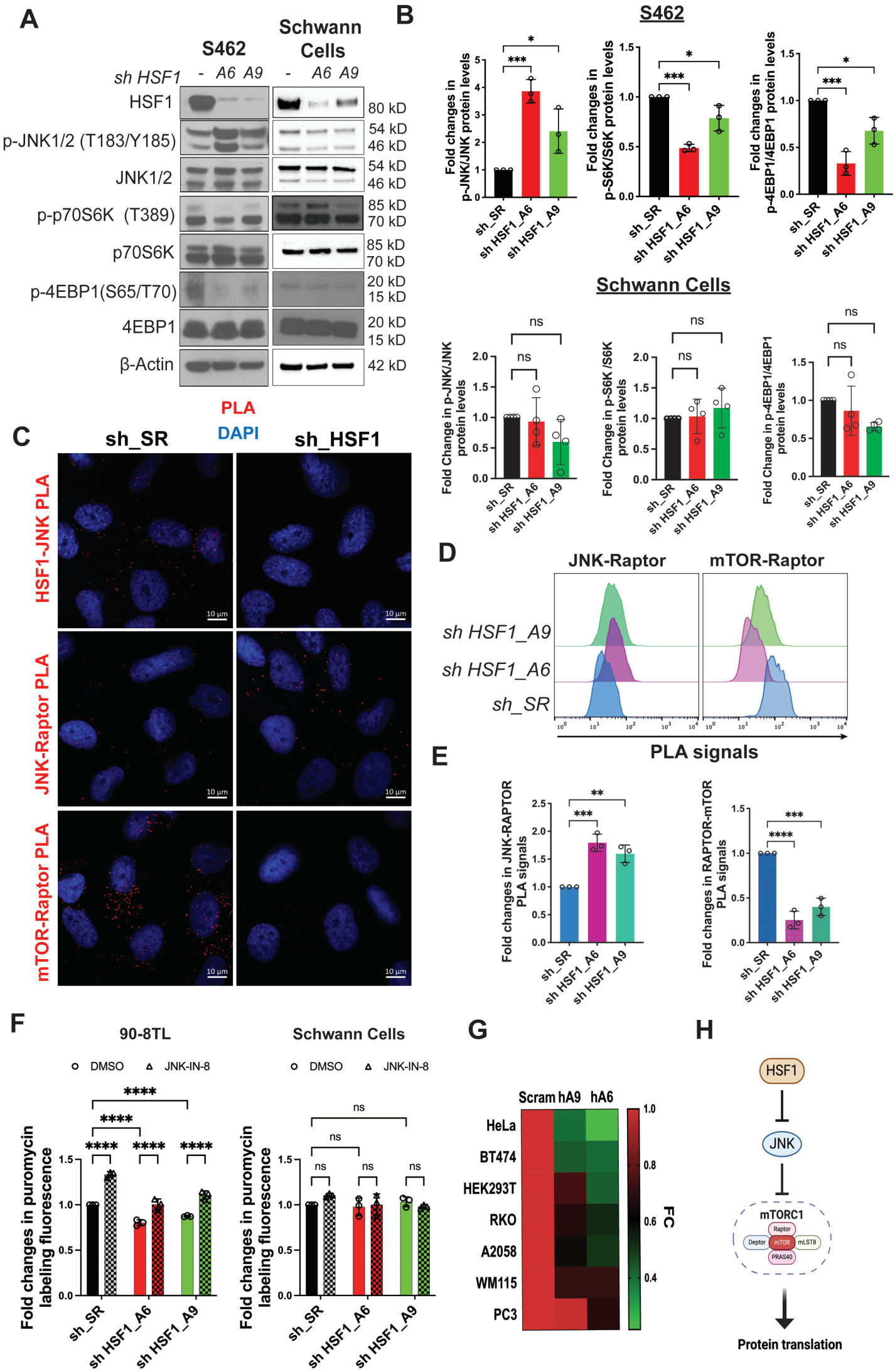
A
S462
Schwann Cells
sh HSF1
- A6 A9
- A6 A9
HSF1
p-JNK1/2 (T183/Y185)
JNK1/2
p-p70S6K (T389)
p70S6K
p-4EBP1(S65/T70)
4EBP1
β-Actin
80 kD
54 kD
46 kD
54 kD
46 kD
85 kD
70 kD
85 kD
70 kD
20 kD
15 kD
20 kD
15 kD
42 kD
B
S462
Fold changes in p-JNK/JNK protein levels
Fold changes in p-S6K/S6K protein levels
Fold changes in p-4EBP1/4EBP1 protein levels
sh_SR
sh HSF1_A6
sh HSF1_A9
Schwann Cells
Fold Change in p-JNK/JNK protein levels
Fold Change in p-S6K /S6K protein levels
Fold Change in p-4EBP1/4EBP1 protein levels
ns
C
PLA
DAPI
sh_SR
sh_HSF1
HSF1-JNK PLA
JNK-Raptor PLA
mTOR-Raptor PLA
10 µm
D
JNK-Raptor
mTOR-Raptor
sh HSF1_A9
sh HSF1_A6
sh_SR
PLA signals
E
Fold changes in JNK-RAPTOR PLA signals
Fold changes in RAPTOR-mTOR PLA signals
sh_SR
sh HSF1_A6
sh HSF1_A9
F
90-8TL
Schwann Cells
DMSO
JNK-IN-8
Fold changes in puromycin labeling fluorescence
sh_SR
sh HSF1_A6
sh HSF1_A9
G
Scram hA9 hA6
HeLa
BT474
HEK293T
RKO
A2058
WM115
PC3
FC
H
HSF1
JNK
mTORC1
Raptor
Deptor
mTOR
mLST8
PRAS40
Protein translation

1025 **Figure 3: JNK senses *HSF1* deficiency to repress mTORC1 and protein translation in**
1026 **MPNST cells.** (A) Detection of JNK activation and mTORC1 inhibition following *HSF1*
1027 depletion in S462 and primary human Schwann cells by immunoblotting. (B) Quantitation of (A)
1028 using Fiji imaging software (mean ± SD, n=3 independent experiments, One-way ANOVA). (C)
1029 Detection of HSF1-JNK, JNK-RAPTOR, and mTOR-RAPTOR interactions by PLA in S462
1030 cells with and without *HSF1* depletion. (D) and (E) Detection and quantitation of JNK-RAPTOR
1031 and mTOR-RAPTOR interactions by PLA flow cytometry in 90-8TL cells (mean ± SD, n=3
1032 independent experiments, One-way ANOVA). (F) Measurement of protein translation rates in
1033 90-8TL and primary human Schwann cells with and without *HSF1* depletion by puromycin
1034 labeling, analyzed by flow cytometry. Cells were treated with 1 μM JNK-IN-8 for 24 hrs before
1035 labeling with 100 nM 6-FAM-dc-puromycin for 30 min (mean ± SD, n=3 independent
1036 experiments, Two-way ANOVA). (G) Heatmap of protein translation rates measured by
1037 puromycin labeling in diverse human cancer cell lines with and without *HSF1* depletion. (H)
1038 Schematic depiction of regulation of protein translation by HSF1.
1039
1040
1041
1042
1043
1044
1045
1046
1047

Figure 4

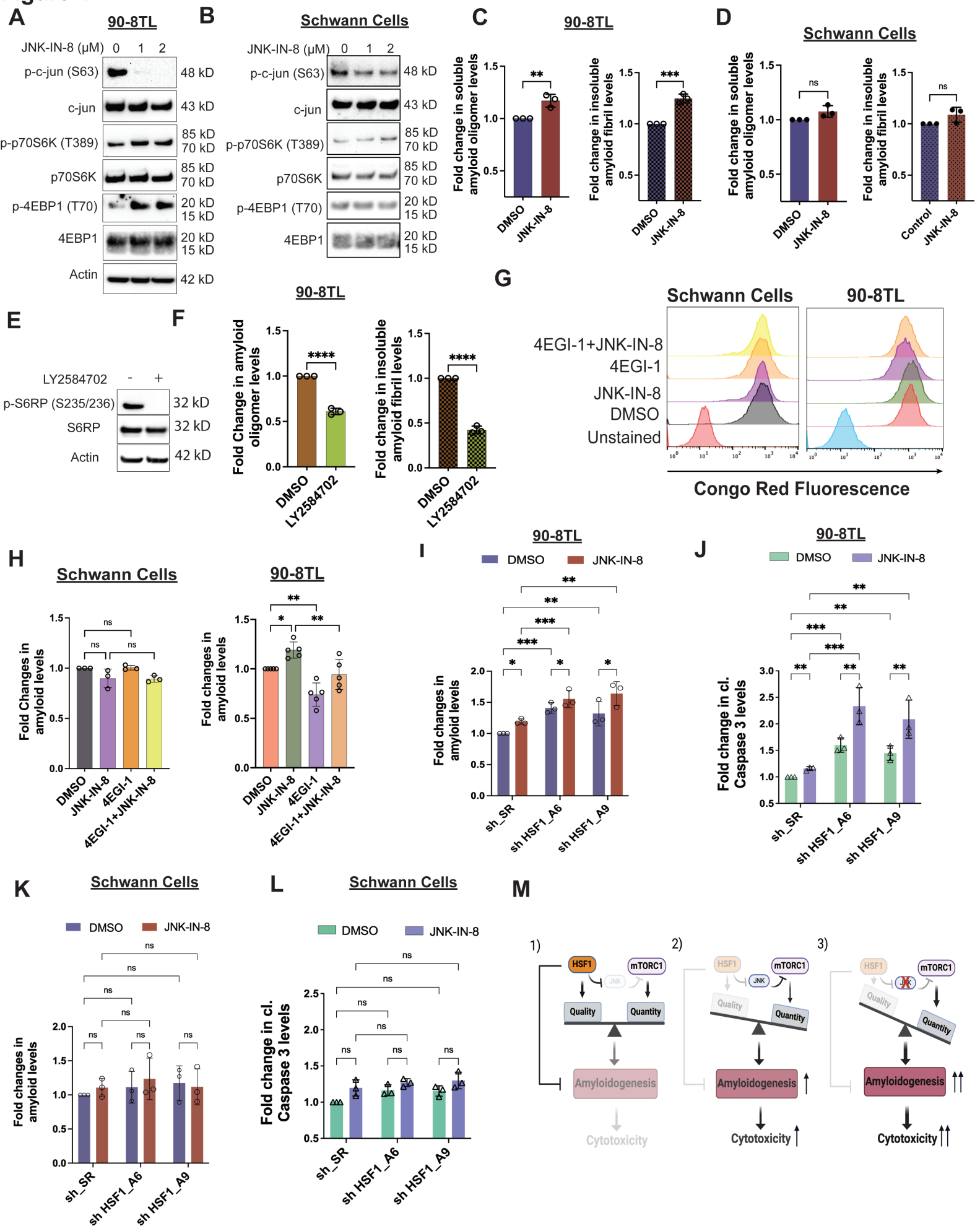
A
90-8TL
JNK-IN-8 (μM) 0 1 2
p-c-jun (S63) 48 kD
c-jun 43 kD
p-p70S6K (T389) 85 kD 70 kD
p70S6K 85 kD 70 kD
p-4EBP1 (T70) 20 kD 15 kD
4EBP1 20 kD 15 kD
Actin 42 kD
B
Schwann Cells
JNK-IN-8 (μM) 0 1 2
p-c-jun (S63) 48 kD
c-jun 43 kD
p-p70S6K (T389) 85 kD 70 kD
p70S6K 85 kD 70 kD
p-4EBP1 (T70) 20 kD 15 kD
4EBP1 20 kD 15 kD
C
90-8TL
Fold change in soluble amyloid oligomer levels
Fold change in insoluble amyloid fibril levels
DMSO
JNK-IN-8
D
Schwann Cells
Fold change in soluble amyloid oligomer levels
Fold change in insoluble amyloid fibril levels
ns
DMSO
JNK-IN-8
Control
E
LY2584702 - +
p-S6RP (S235/236) 32 kD
S6RP 32 kD
Actin 42 kD
F
90-8TL
Fold Change in amyloid oligomer levels
Fold change in insoluble amyloid fibril levels
DMSO
LY2584702
G
Schwann Cells
90-8TL
4EGI-1+JNK-IN-8
4EGI-1
JNK-IN-8
DMSO
Unstained
Congo Red Fluorescence
H
Schwann Cells
90-8TL
Fold Changes in amyloid levels
Fold changes in amyloid levels
DMSO
JNK-IN-8
4EGI-1
4EGI-1+JNK-IN-8
I
90-8TL
DMSO
JNK-IN-8
Fold changes in amyloid levels
sh_SR
sh HSF1_A6
sh HSF1_A9
J
90-8TL
DMSO
JNK-IN-8
Fold change in cl. Caspase 3 levels
sh_SR
sh HSF1_A6
sh HSF1_A9
K
Schwann Cells
DMSO
JNK-IN-8
Fold changes in amyloid levels
sh_SR
sh HSF1_A6
sh HSF1_A9
L
Schwann Cells
DMSO
JNK-IN-8
Fold change in cl. Caspase 3 levels
sh_SR
sh HSF1_A6
sh HSF1_A9
M
1)
2)
3)
HSF1
mTORC1
JNK
Quality
Quantity
Amyloidogenesis
Cytotoxicity

1048 **Figure 4: Protein translation is causally related to amyloidogenesis in MPNST cells.**
1049 (A) and (B) Detection of mTORC1 stimulation following JNK inhibition in 90-8TL and
1050 immortalized human Schwann cells by immunoblotting. Cells were treated with JNK-IN-8 for 2
1051 days. (C) and (D) Quantitation of soluble AOs and insoluble AFs by ELISA in 90-8TL and
1052 human Schwann cells with and without 3 μM JNK-IN-8 treatment for 3 days (mean ± SD, n=3
1053 independent experiments, Student's t test). (E) Detection of LY2584702-mediated S6K
1054 inhibition in 90-8TL cells by immunoblotting. Cells were treated with 20 μM LY2584702 for 2
1055 days. (F) Quantitation of soluble AOs and insoluble AFs by ELISA in 90-8TL cells with and
1056 without 20 μM LY2584702 treatment for 2 days (mean ± SD, n=3 independent experiments,
1057 Student's t test). (G) CR staining of 90-8TL and immortalized human Schwann cells with and
1058 without JNK-IN-8 and 4EGI-1 treatment, detected by flow cytometry. (H) Quantitation of (G)
1059 using the median fluorescence intensity (mean ± SD, n=3 independent experiments, One-way
1060 ANOVA). (I) Quantitation of amyloids by CR staining in 90-8TL cells with and without *HSF1*
1061 depletion and 3 μM JNK-IN-8 treatment (mean ± SD, n=3 independent experiments, Two-way
1062 ANOVA). (J) Quantitation of caspase 3 cleavage by ELISA in 90-8TL cells with and without
1063 *HSF1* depletion and 3 μM JNK-IN-8 treatment (mean ± SD, n=3 independent experiments, Two-
1064 way ANOVA). (K) Quantitation of amyloids by CR staining in immortalized human Schwann
1065 cells with and without *HSF1* depletion and 3 μM JNK-IN-8 treatment (mean ± SD, n=3
1066 independent experiments, Two-way ANOVA). (L) Quantitation of caspase 3 cleavage by ELISA
1067 in immortalized human Schwann cells with and without *HSF1* depletion and 3 μM JNK-IN-8
1068 treatment (mean ± SD, n=3 independent experiments, Two-way ANOVA). (M) Schematic
1069 depiction of the adaptation of MPNST cells to *HSF1* depletion by activating JNK to suppress
1070 mTORC1 and protein translation, thereby alleviating amyloidogenesis and cytotoxicity.

Figure 5

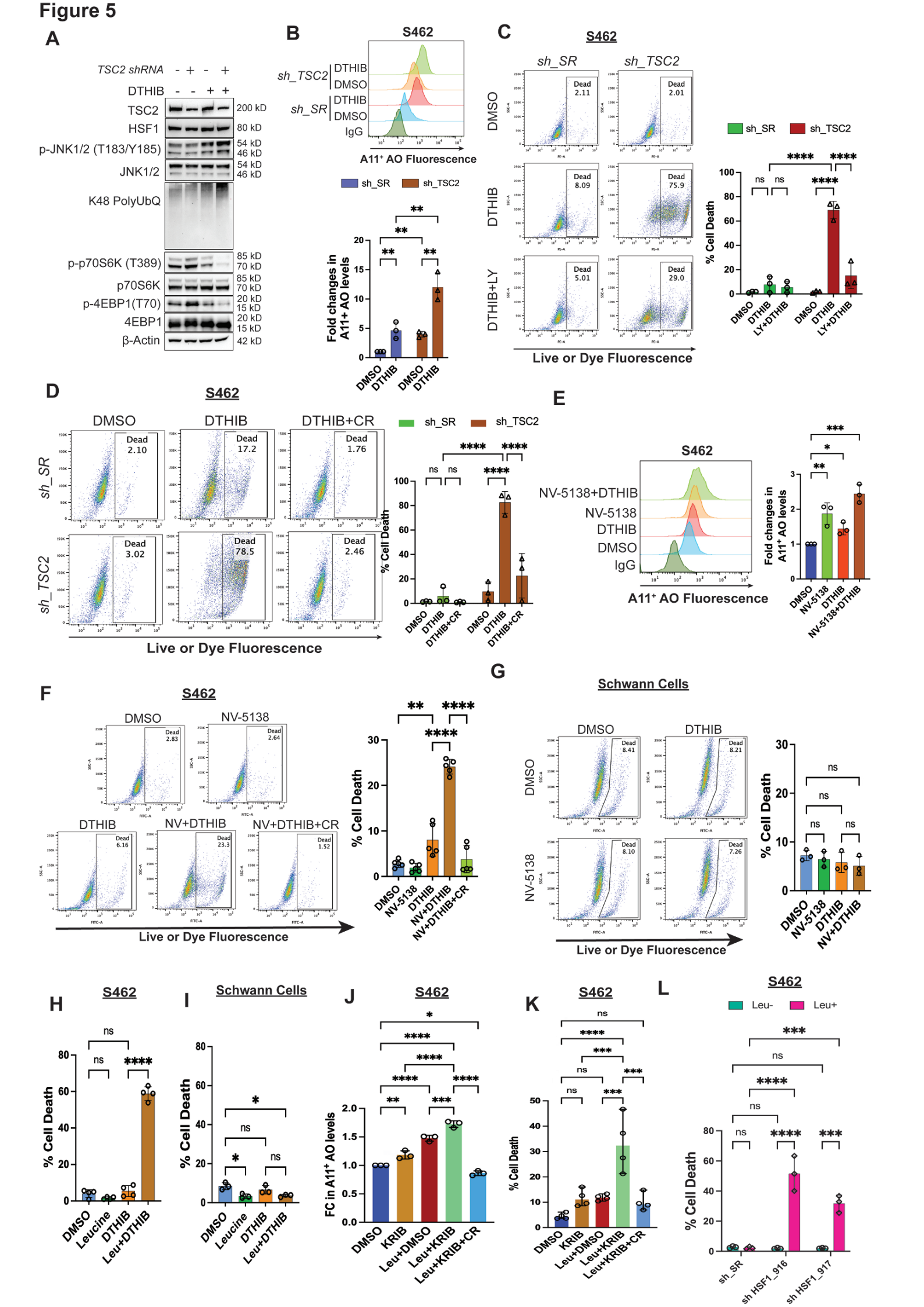
A
TSC2 shRNA - + - +
DTHIB - - + +
TSC2
HSF1
p-JNK1/2 (T183/Y185)
JNK1/2
K48 PolyUbQ
p-p70S6K (T389)
p70S6K
p-4EBP1(T70)
4EBP1
β-Actin
200 kD
80 kD
54 kD
46 kD
85 kD
70 kD
20 kD
15 kD
42 kD
B
S462
sh_TSC2
DTHIB
DMSO
sh_SR
IgG
A11+ AO Fluorescence
sh_SR
sh_TSC2
Fold changes in A11+ AO levels
DMSO
DTHIB
C
S462
sh_SR
sh_TSC2
DMSO
DTHIB
DTHIB+LY
Dead 2.11
Dead 2.01
Dead 8.09
Dead 75.9
Dead 5.01
Dead 29.0
Live or Dye Fluorescence
% Cell Death
LY+DTHIB
D
S462
DMSO
DTHIB
DTHIB+CR
sh_SR
sh_TSC2
Dead 2.10
Dead 17.2
Dead 1.76
Dead 3.02
Dead 78.5
Dead 2.46
Live or Dye Fluorescence
% Cell Death
E
S462
NV-5138+DTHIB
NV-5138
DTHIB
DMSO
IgG
A11+ AO Fluorescence
Fold changes in A11+ AO levels
F
S462
DMSO
NV-5138
DTHIB
NV+DTHIB
NV+DTHIB+CR
Dead 2.83
Dead 2.64
Dead 6.16
Dead 23.3
Dead 1.52
Live or Dye Fluorescence
% Cell Death
G
Schwann Cells
DMSO
DTHIB
NV-5138
Dead 8.41
Dead 8.21
Dead 8.10
Dead 7.26
Live or Dye Fluorescence
% Cell Death
H
S462
% Cell Death
DMSO
Leucine
DTHIB
Leu+DTHIB
I
Schwann Cells
% Cell Death
J
S462
FC in A11+ AO levels
DMSO
KRIB
Leu+DMSO
Leu+KRIB
Leu+KRIB+CR
K
S462
% Cell Death
L
S462
Leu-
Leu+
% Cell Death
sh_SR
sh HSF1_916
sh HSF1_917

1071 **Figure 5: mTORC1 stimulation aggravates the amyloidogenesis and cytotoxicity elicited by**
1072 **HSF1 inhibition.** (A) Immunoblotting detection of JNK activation, mTORC1 activity, and
1073 protein polyubiquitination in S462 cells following stable *TSC2* knockdown and/or HSF1
1074 inhibition by 10 μM DTHIB for 3 days. (B) Quantitation of soluble AOs by flow cytometry
1075 using A11 antibody staining in S462 cells with and without *TSC2* knockdown and 10 μM
1076 DTHIB treatment (mean ± SD, n=3 independent experiments, Two-way ANOVA). (C)
1077 Quantitation of cytotoxicity by flow cytometry using Live-or-Dye stains in S462 cells with and
1078 without stable *TSC2* knockdown and DTHIB (10 μM) or combined DTHIB and LY2584702 (20
1079 μM) treatment (mean ± SD, n=3 independent experiments, Two-way ANOVA). Cells were pre-
1080 treated with LY2584702 for 1 day followed by DTHIB treatment for another 3 days. (D)
1081 Quantitation of cytotoxicity by flow cytometry using Live-or-Dye stains in S462 cells with and
1082 without stable *TSC2* knockdown and DTHIB (10 μM) or combined DTHIB and CR (30 μM)
1083 treatment (mean ± SD, n=3 independent experiments, Two-way ANOVA). Cells were pre-
1084 treated with CR for 1 day followed by DTHIB treatment for another 3 days. (E) Quantitation of
1085 soluble AOs by flow cytometry using A11 antibody staining in S462 cells with and without 500
1086 μM NV-5138 stimulation and 10 μM DTHIB treatment (mean ± SD, n=3 independent
1087 experiments, One-way ANOVA). (F) Quantitation of cytotoxicity by flow cytometry using Live-
1088 or-Dye stains in S462 cells with and without 500 μM NV-5138 stimulation and 10 μM DTHIB
1089 or combined DTHIB and CR treatment (mean ± SD, n=5 independent experiments, One-way
1090 ANOVA). (G) Quantitation of cytotoxicity by flow cytometry using Live-or-Dye stains in
1091 immortalized human Schwann cells with and without 500 μM NV-5138 stimulation and 10 μM
1092 DTHIB treatment (mean ± SD, n=3 independent experiments, One-way ANOVA). (H)
1093 Quantitation of cytotoxicity by flow cytometry using Live-or-Dye stains in S462 cells with and

1094 without 500 μM L-leucine stimulation and 10 μM DTHIB treatment (mean ± SD, n=4
1095 independent experiments, One-way ANOVA). (I) Quantitation of cytotoxicity by flow cytometry
1096 using Live-or-Dye stains in immortalized human Schwann cells with and without 500 μM L-
1097 leucine stimulation and 10 μM DTHIB treatment (mean ± SD, n=3 independent experiments,
1098 One-way ANOVA). (J) Quantitation of soluble AOs by ELISA in S462 cells treated with and
1099 without 800 μM L-leucine and 20 μM KRIBB11 or 30 μM CR (mean ± SD, n=3 independent
1100 experiments, One-way ANOVA). (K) Quantitation of cytotoxicity by flow cytometry using Live-
1101 or-Dye stains in S462 cells treated as above (mean ± SD, n=4 independent experiments, One-
1102 way ANOVA). (L) Quantitation of cytotoxicity by flow cytometry using Live-or-Dye stains in
1103 S462 cells stably expressing inducible shRNAs with and without L-leucine stimulation. Cells
1104 were first cultured with or without 1.2 mM L-leucine for 2 days, followed by addition of 20
1105 ng/ml doxycycline for 7 days (mean ± SD, n=3 independent experiments, One-way ANOVA).
1106
1107
1108
1109
1110
1111
1112
1113
1114
1115
1116

Figure 6

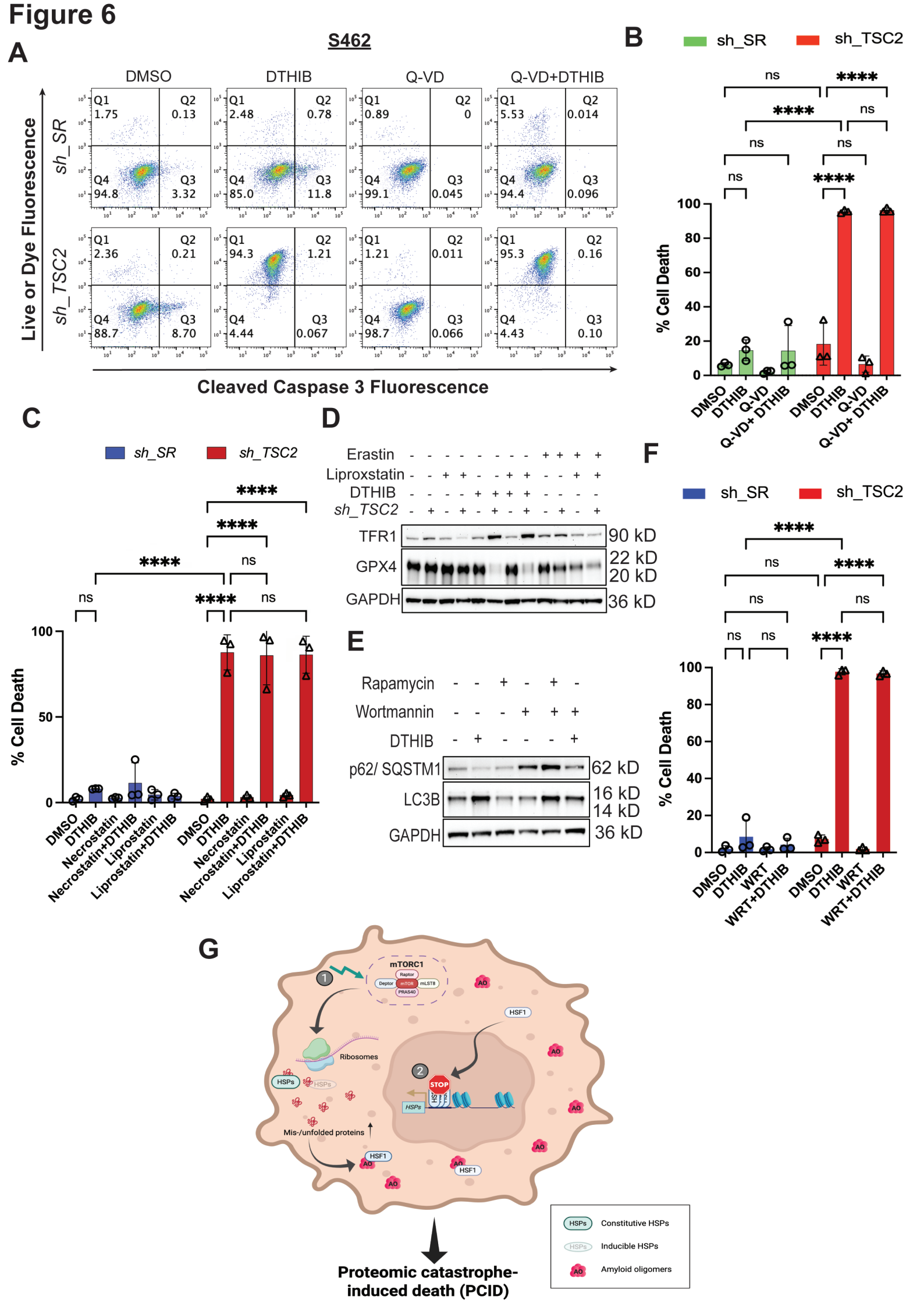
A
S462
DMSO
DTHIB
Q-VD
Q-VD+DTHIB
sh_SR
sh_TSC2
Q1 1.75
Q2 0.13
Q4 94.8
Q3 3.32
Q1 2.48
Q2 0.78
Q4 85.0
Q3 11.8
Q1 0.89
Q2 0
Q4 99.1
Q3 0.045
Q1 5.53
Q2 0.014
Q4 94.4
Q3 0.096
Q1 2.36
Q2 0.21
Q4 88.7
Q3 8.70
Q1 94.3
Q2 1.21
Q4 4.44
Q3 0.067
Q1 1.21
Q2 0.011
Q4 98.7
Q3 0.066
Q1 95.3
Q2 0.16
Q4 4.43
Q3 0.10
Live or Dye Fluorescence
Cleaved Caspase 3 Fluorescence
B
sh_SR
sh_TSC2
% Cell Death
DMSO
DTHIB
Q-VD
Q-VD+ DTHIB
C
sh_SR
sh_TSC2
% Cell Death
DMSO
DTHIB
Necrostatin
Necrostatin+DTHIB
Liprostatin
Liprostatin+DTHIB
D
Erastin
Liproxstatin
DTHIB
sh_TSC2
TFR1
GPX4
GAPDH
90 kD
22 kD
20 kD
36 kD
E
Rapamycin
Wortmannin
DTHIB
p62/ SQSTM1
LC3B
GAPDH
62 kD
16 kD
14 kD
36 kD
F
sh_SR
sh_TSC2
% Cell Death
DMSO
DTHIB
WRT
WRT+DTHIB
G
mTORC1
Raptor
Deptor
mTOR
mLST8
PRAS40
HSF1
Ribosomes
HSPs
STOP
HSPs
Mis-/unfolded proteins
Constitutive HSPs
Inducible HSPs
Amyloid oligomers
Proteomic catastrophe-induced death (PCID)

1117 **Figure 6: Concurrent HSF1 inhibition and mTORC1 stimulation instigate widespread non-**
1118 **apoptotic cell death.** (A) and (B) Quantitation of cytotoxicity by flow cytometry using Live-or-
1119 Dye stains combined with cleaved caspase 3 (Asp175) antibody staining. S462 cells with and
1120 without stable *TSC2* knockdown were treated with DMSO, 10 μM DTHIB, or combined DTHIB
1121 and 30 μM Q-VD-OPh (mean ± SD, n=3 independent experiments, Two-way ANOVA). (C)
1122 Quantitation of cytotoxicity by flow cytometry using Live-or-Dye stains in S462 cells with and
1123 without stable *TSC2* knockdown. Cells were treated with 10 μM DTHIB alone or co-treated with
1124 10 μM DTHIB and 30 μM Necrostatin-1 or 20 μM Liproxstatin-1 for 3 days (mean ± SD, n=3
1125 independent experiments, Two-way ANOVA). (D) Immunoblotting detection of ferroptosis
1126 markers in S462 cells with and without stable *TSC2* knockdown treated with 10 μM DTHIB
1127 alone or co-treated with 10 μM DTHIB and 20 μM liproxstatin-1 for 3 days. Erastin was
1128 included as a positive control to induce canonical ferroptosis. (E) Immunoblotting detection of
1129 autophagy markers in S462 cells with stable *TSC2* knockdown treated with 10 μM DTHIB alone
1130 or co-treated with 10 μM DTHIB and 3 μM wortmannin for 3 days. Rapamycin was included as
1131 a positive control to induce autophagy. (F) Quantitation of cytotoxicity by flow cytometry using
1132 Live-or-Dye stains in S462 cells with and without stable *TSC2* knockdown. Cells were treated
1133 with 10 μM DTHIB alone or co-treated with 10 μM DTHIB and 3 μM wortmannin for 3 days
1134 (mean ± SD, n=3 independent experiments, Two-way ANOVA). (G) Schematic depiction of
1135 instigation of cell death by severe proteomic imbalance, owing to simultaneous mTORC1
1136 stimulation (❶) and HSF1 inhibition (❷). In cancer cells, constitutive HSF1 activation
1137 provides extra chaperoning capacity to cope with elevated protein misfolding, partly due to
1138 enhanced protein synthesis and widespread genetic mutations. Nevertheless, amyloids still
1139 emerge, although at low levels. Importantly, HSF1 can neutralize highly toxic amyloid

oligomers, averting lethal consequences. By contrast, HSF1 inhibition diminishes chaperoning capacity, insufficient to counterbalance the robust protein translation. mTORC1 stimulation further aggravates this proteomic imbalance, which, in turn, promotes amyloidogenesis and proteomic catastrophe. In consequence, the amounts of amyloid oligomers surpass the neutralizing capacity of HSF1, leading to cell death; nonetheless, it remains unclear how this proteomic catastrophe-induced death (PCID) occurs.

Figure 7

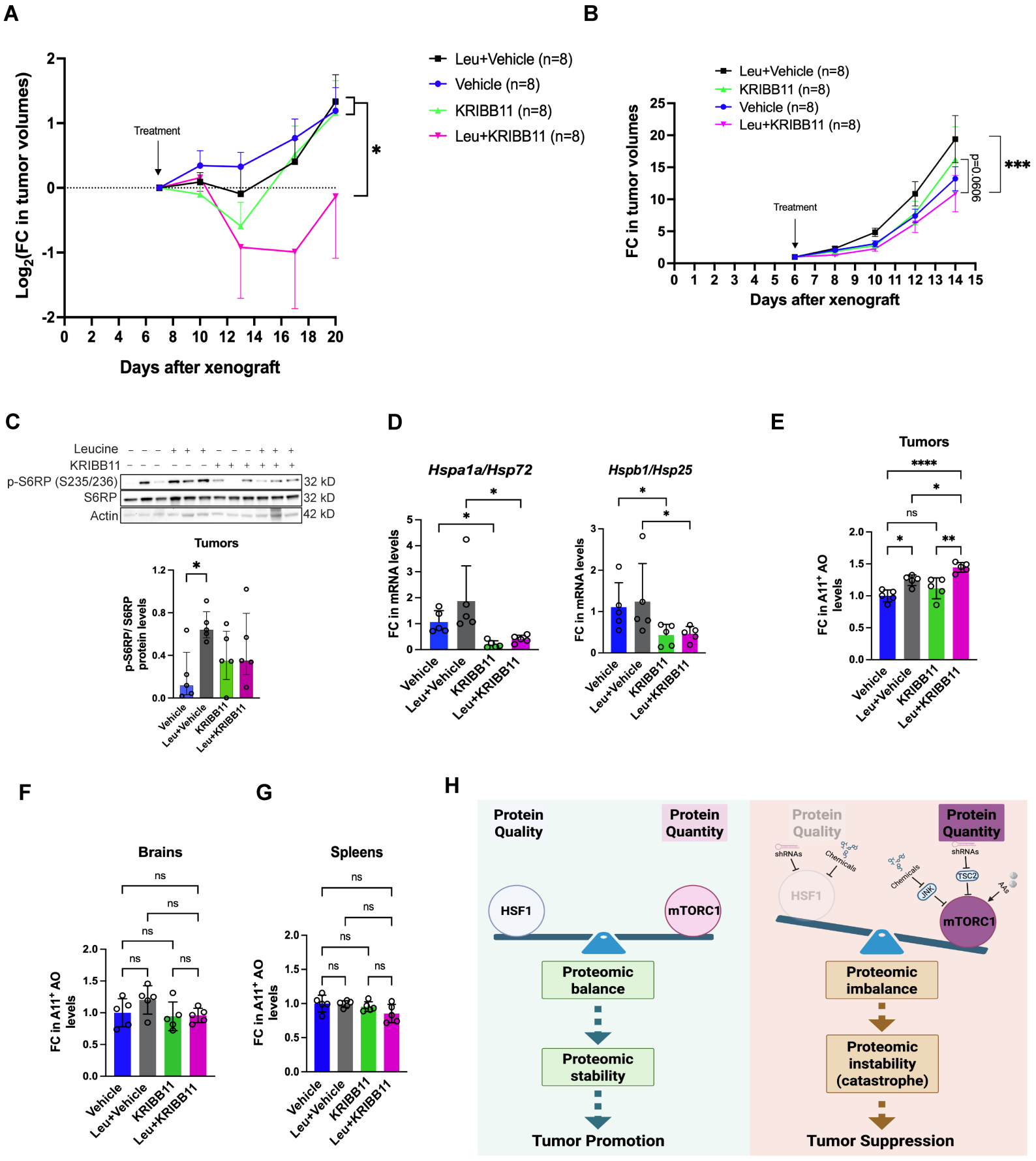
A
Log2(FC in tumor volumes)
Treatment
Days after xenograft
Leu+Vehicle (n=8)
Vehicle (n=8)
KRIBB11 (n=8)
Leu+KRIBB11 (n=8)
B
FC in tumor volumes
Treatment
Days after xenograft
p=0.0606
C
Leucine
KRIBB11
p-S6RP (S235/236)
S6RP
Actin
32 kD
32 kD
42 kD
Tumors
p-S6RP/ S6RP protein levels
Vehicle
Leu+Vehicle
KRIBB11
Leu+KRIBB11
D
Hspa1a/Hsp72
Hspb1/Hsp25
FC in mRNA levels
E
Tumors
FC in A11+ AO levels
F
Brains
G
Spleens
H
Protein Quality
Protein Quantity
HSF1
mTORC1
Proteomic balance
Proteomic stability
Tumor Promotion
shRNAs
Chemicals
JNK
TSC2
Akt
Proteomic imbalance
Proteomic instability (catastrophe)
Tumor Suppression

1163 **Figure 7: Concurrent HSF1 inhibition and mTORC1 stimulation suppress *in vivo* tumor**
1164 **growth.** (A) Combined KRIBB11 treatment and L-leucine stimulation impaired the *in vivo*
1165 growth of xenografted S462 human MPNST cells in NIH-III nude mice (mean ± SEM, n=8 mice
1166 per group, $\log_2$ transformation for Two-way ANOVA). (B) Combined KRIBB11 treatment and
1167 L-leucine stimulation impeded the *in vivo* growth of xenografted B16-F10 murine melanoma
1168 cells in C57BL/6J mice (mean ± SEM, n=8 mice per group, $\log_2$ transformation for Two-way
1169 ANOVA). (C) Quantitation of phospho-S6RP by immunoblotting in treated melanomas. Images
1170 show representative 3 tumors each group (mean ± SEM, n=5 tumors per group, One-way
1171 ANOVA). (D) Quantitation of *Hsp72* and *Hsp25* mRNAs in treated melanomas by RT-qPCR
1172 (mean ± SD, n=5 tumors per group, One-way ANOVA). (E) Quantitation of soluble AOs in
1173 treated B16F10 melanomas by ELISA ((mean ± SD, n=5 tumors per group, One-way ANOVA).
1174 (F) and (G) Quantitation of soluble AOs in brains and spleens from treated C57BL/6J mice by
1175 ELISA (mean ± SD, n=5 brains or spleens per group, One-way ANOVA). (H) Schematic
1176 depiction of the concept of provoking proteomic catastrophe to combat malignancy. On the one
1177 hand, in cancer cells, mTORC1 is inevitably activated to stimulate protein translation, markedly
1178 augmenting protein quantity. On the other hand, the extra chaperoning capacity governed by
1179 HSF1, albeit dispensable for normal life, becomes necessary to ensure sufficient protein quality
1180 in cancer cells, thereby counterbalancing augmented protein quantity and suppressing proteomic
1181 instability. Thus, proteomic balance promotes malignant growth. By contrast, disrupting
1182 proteomic balance, through HSF1 inhibition, is sufficient to elicit proteomic instability and
1183 tumor suppression. However, simultaneous mTORC1 stimulation can remarkably drive
1184 proteomic imbalance, causing proteomic catastrophe that leads to tumor suppression.